SUMOylation represses SnRK1 signaling in Arabidopsis

Crozet, P.*[1], Margalha, L.*[1], Butowt, R.[1,2], Fernandes, N.[1], Elias, A.[1], Orosa, B.[3], Tomanov, K.[4], Teige, M.[5], Bachmair, A.[4], Sadanandom, A.[3], and Baena-González, E.[1#]

*Equal contribution

[1]Instituto Gulbenkian de Ciência, Rua da Quinta Grande 6, 2780-156, Oeiras, Portugal

[2]Present address, Department of Molecular Cell Genetics, L. Rydygier Collegium Medicum, Nicolaus Copernicus University, Curie-Sklodowskiej 9, 85-093 Bydgoszcz, Poland

[3]School of Biological and Biomedical Sciences, University of Durham, Durham, UK

[4]Department of Biochemistry and Cell Biology, Max F. Perutz Laboratories, Vienna BioCenter, University of Vienna, A-1030 Vienna, Austria

[5]Department of Ecogenomics and Systems Biology, University of Vienna, Althanstr. 14, A-1090, Vienna, Austria

[#]Corresponding Author

Keywords: SUMOylation; ubiquitination; SNF1-related protein kinase (SnRK1); energy signaling; stress; SIZ1; *Arabidopsis thaliana*

Short Title: SUMOylation represses SnRK1 signaling

Word count: 7635

(1) Summary: 167

(2) Significance statement: 65

(3) Introduction: 873

(4) Results: 2601

(5) Discussion: 1388

(6) Experimental procedures: 986

(7) Accession numbers: 55

(8) Acknowledgements: 91

(9) References: 1894

(10) Figure legends: 1286

Email addresses:

pcrozet@igc.gulbenkian.pt

lrduarte@igc.gulbenkian.pt

r.butowt@cm.umk.pl

nfernandes@igc.gulbenkian.pt

celias@igc.gulbenkian.pt

beatriz.orosa@durham.ac.uk

konstantin.tomanov@univie.ac.at

Markus.Teige@Univie.ac.at

andreas.bachmair@univie.ac.at

ari.sadanandom@durham.ac.uk

ebaena@igc.gulbenkian.pt

SUMMARY

The SnRK1 protein kinase balances cellular energy levels in accordance with extracellular conditions and is thereby key for plant stress tolerance. In addition, SnRK1 has been implicated in numerous growth and developmental processes from seed filling and maturation to flowering and senescence. Despite its importance, the mechanisms that regulate SnRK1 activity are poorly understood. Here, we demonstrate that the SnRK1 complex is SUMOylated on multiple subunits and identify SIZ1 as the E3 SUMO ligase responsible for this modification. We further show that SnRK1 is ubiquitinated in a SIZ1-dependent manner, causing its degradation through the proteasome. In consequence, SnRK1 degradation is deficient in *siz1-2* mutants, leading to its accumulation and hyperactivation of SnRK1 signaling. Finally, SnRK1 degradation is strictly dependent on its activity, as inactive SnRK1 variants are aberrantly stable but recover normal degradation when expressed as SUMO mimetics. Altogether, our data suggest that active SnRK1 triggers its own SUMOylation and degradation, establishing a negative feedback loop that attenuates SnRK1 signaling and prevents detrimental hyperactivation of stress responses.

SIGNIFICANCE STATEMENT

The SnRK1 protein kinase is crucial for tolerance to environmental stress and for a wide range of plant growth and developmental processes, but how its activity is regulated is unknown. Here, we demonstrate that SnRK1 activity causes its own SUMOylation and subsequent ubiquitination and proteasomal degradation, thus establishing a negative feedback loop that attenuates SnRK1 signaling and potentially prevents detrimental sustained activation of stress responses.

INTRODUCTION

The plant Snf1-related Protein Kinase 1 (SnRK1) is a central component of a sophisticated signaling network that translates the plant carbon status into defense, growth and developmental decisions (Lastdrager *et al.* 2014). SnRK1 downregulates growth-related processes, partly through inhibition of major biosynthetic enzymes of carbon and nitrogen metabolism (Polge *et al.* 2008; Sugden *et al.* 1999). In addition, it controls the expression of over a thousand genes involved in metabolism, signaling, transcription, stress tolerance, transport and growth (Baena-Gonzalez *et al.* 2007; Baena-Gonzalez and Sheen 2008). The coordinated metabolic and transcriptional regulation by SnRK1 contributes to maintaining cellular homeostasis during stress, thereby promoting tolerance and survival (Baena-Gonzalez *et al.* 2007; Hao *et al.* 2003; Lee *et al.* 2009; Lin *et al.* 2014; Lovas *et al.* 2003; Schwachtje *et al.* 2006). SnRK1 has also been implicated in ABA hormone signaling as well as in numerous developmental processes from seed filling, maturation, and germination to reproduction and senescence (Ananieva *et al.* 2008; Baena-Gonzalez *et al.* 2007; Bhalerao *et al.* 1999; Coello *et al.* 2012; Jossier *et al.* 2009; Lee *et al.* 2008; Lee *et al.* 2009; Lin *et al.* 2014; Lu *et al.* 2007; Radchuk *et al.* 2010; Radchuk *et al.* 2006; Rodrigues *et al.* 2013; Schwachtje *et al.* 2006; Thelander *et al.* 2004; Tsai and Gazzarrini 2012). Finally, transient systemic silencing of SnRK1 results in growth arrest and premature senescence, highlighting the centrality of the SnRK1 system for normal plant growth and development (Baena-Gonzalez *et al.* 2007; Thelander *et al.* 2004).

SnRK1 is the plant ortholog of the budding yeast Snf1 (Sucrose-non-fermenting 1) and mammalian AMPK (AMP-activated protein kinase). All three enzymes function as heterotrimeric complexes composed of an α-catalytic and two β- and γ-regulatory subunits, and in all cases kinase activity requires phosphorylation of a conserved T-loop threonine in the α-subunit (Baena-Gonzalez *et al.* 2007; Crozet *et al.* 2014; Polge and Thomas 2007).

However, the intimate connection between T-loop phosphorylation in response to energy deprivation and kinase activation observed in SNF1 and AMPK is not established in plants, where additional regulatory mechanisms may be operating (Baena-Gonzalez *et al.* 2007; Coello *et al.* 2012; Fragoso *et al.* 2009; Rodrigues *et al.* 2013). Furthermore, SnRK1 kinase activity appears unchanged under conditions that induce SnRK1 signaling as well as in *pp2c* mutants that display deficient repression of the SnRK1 pathway (Baena-Gonzalez *et al.* 2007; Rodrigues *et al.* 2013). Finally, the plant enzyme has incorporated unique regulatory subunits and other distinct features, presumably to respond to plant-specific signals and/or to perform plant-specific functions (Crozet *et al.* 2014; Emanuelle *et al.* 2015; Polge and Thomas 2007). These studies reveal the atypical nature of the plant kinase and underscore our lack of knowledge on the factors that determine the signaling lifetime of such a central component.

SUMO (Small Ubiquitin-like Modifier) is a small protein (about 12kDa) that is post-translationally conjugated to target proteins in a reversible manner to regulate crucial biological processes. SUMOylation is required for normal growth and development, and consequently, mutants defective in the SUMO pathway are either lethal or display strong phenotypes (Geiss-Friedlander and Melchior 2007; Saracco *et al.* 2007). In addition, exposure to environmental or metabolic stresses induces a dramatic accumulation of SUMO-conjugates, constituting what is considered to be a cellular protective response in all eukaryotes (Guo and Henley 2014). Accordingly, many SUMO targets identified in Arabidopsis are stress-related components (Elrouby and Coupland 2010; Miller *et al.* 2010) and SUMOylation is important for a wide range of plant stress responses (Castro *et al.* 2012). SUMOylation has been ascribed very diverse biochemical functions, including changes in stability, activity, and subcellular localization, primarily through the modulation of protein interactions (Jentsch and Psakhye 2013).

SUMOylation requires the maturation of the SUMO moiety by a SUMO protease, exposing a characteristic C-terminal di-glycine motif (Geiss-Friedlander and Melchior 2007). Mature SUMO is then activated by the SUMO activating enzyme E1 enzyme [SAE1/2 in Arabidopsis (Park *et al.* 2011)], through the formation of a thioester bond, and transferred to the SUMO conjugating enzyme (E2 enzyme, SCE1 in Arabidopsis) through a transthiolation reaction. Finally, SCE conjugates SUMO to a target lysine, either alone or with the help of a SUMO E3 ligase (SIZ1 and HPY2 in Arabidopsis). Substrates can carry single SUMO moieties or SUMO polymers, and in Arabidopsis, two SUMO E4 ligases were recently implicated in the assembly of such SUMO chains (Tomanov *et al.* 2014). SUMO chains may have a role on their own (Ulrich 2008), but can also trigger ubiquitination *via* SUMO-targeted ubiquitin ligases (STUbLs), hence targeting the protein for proteasomal degradation (Elrouby *et al.* 2013; Praefcke *et al.* 2012).

A proteome-wide screen previously identified SnRK1α1 as an interactor of SCE1 (Elrouby and Coupland 2010). In contrast to ubiquitination, where substrate specificity is provided by the E3 ligase, SUMO substrates can be directly recognized and bound on their target lysine by the E2 conjugation enzyme (Geiss-Friedlander and Melchior 2007; Park *et al.* 2011), and hence the SnRK1α1-SCE1 interaction suggests that SnRK1α1 may be a target of SUMOylation. Here, we demonstrate that the SnRK1 complex is SUMOylated by the SIZ1 E3 SUMO ligase, resulting in its ubiquitination and proteasomal degradation. Importantly, SUMO-dependent proteolytic removal targets exclusively active SnRK1, suggesting that SUMOylation acts as a safeguard to avoid sustained activation of stress responses.

RESULTS

The SnRK1 complex is SUMOylated

As a first step to test whether SnRK1 is a target of SUMOylation, we confirmed the reported SnRK1α1-SCE1 interaction in a yeast-two-hybrid assay (Y2H; Figure S1) and found that it occurs mostly through the SnRK1α1 regulatory domain (RD). However, a weaker interaction with the SnRK1α1 kinase domain (KD) could also be detected in less stringent selection media.

To investigate whether SnRK1α1-SCE1 interaction results into SnRK1 SUMOylation, we initially employed an heterologous system in which the Arabidopsis SUMOylation machinery is reconstituted and co-expressed with individual potential substrates in *E. coli* (Okada *et al.* 2009). In the presence of mature SUMO1 or mature SUMO3 (SUMO-GG), SnRK1α1 displayed a clear SUMOylation signal that was absent in the corresponding non-conjugatable isoforms (SUMO-AA), used as negative controls (Figure 1A). We could also observe SUMOylation of SnRK1β1, SnRK1β2 (Figure 1A), and SnRK1γ (Figure S2A), although in the case of the latter the functional connection to SnRK1 remains uncertain (Emanuelle *et al.* 2015; Ramon *et al.* 2013). The only tested subunit for which SUMOylation was not detected was SnRK1βγ (Figure 1A), recently proposed to be the only γ-type subunit of the SnRK1 complex (Emanuelle *et al.* 2015; Ramon *et al.* 2013). These results show that in this *E. coli* system SUMOylation occurs specifically on several components of the SnRK1 complex.

To determine if SUMOylation of SnRK1 also occurs *in planta*, we made use of a *snrk1α1* knockout mutant complemented with SnRK1α1-GFP driven by its own upstream and downstream regulatory regions (*pSnRK1α1::SnRK1α1-GFP::tSnRK1α1*/*snrk1α1-3*; hereafter referred as *SnRK1α1-GFP*; Figure S3). GFP immunoprecipitation followed by Western blot analyses with an anti-SUMO1 antibody revealed a massive accumulation of SUMO1 conjugates in immunoprecipitates from *SnRK1α1-GFP* plants but not from control plants expressing *35S::GFP* (Figure 1B). Interestingly, SUMO1 conjugates associated with

SnRK1α1-GFP were not resolved as distinct bands, but rather as a high molecular weight (hMW) ladder, suggesting the formation of (poly)SUMO chains and/or the SUMOylation of multiple residues. This was further supported by the presence of hMW SnRK1α1 forms in the SnRK1α1 immunoblot (Figure 1B, middle panel). Immunodetection with SnRK1β1 and SnRK1βγ antibodies confirmed the association of these subunits with SnRK1α1-GFP (Figure 1C). We could detect hMW forms of SnRK1β1 but not of SnRK1βγ, suggesting that only the former is SUMOylated *in planta*, in accordance with the results obtained in the *E. coli* SUMOylation system (Figure 1A). To assess the contribution of the β–subunit(s) to SnRK1 SUMOylation, we generated a transgenic line expressing a truncated SnRK1α1 variant lacking the KA1 domain (Rodrigues *et al.* 2013), required for the interaction with the β and γ regulatory subunits (Bhalerao *et al.* 1999; Kleinow *et al.* 2000) (*pSnRK1α1::SnRK1α1ΔKA1-GFP::tSnRK1α1*/*snrk1α1-3*; hereafter referred as *SnRK1α1ΔKA1-GFP*, Figure S3). As expected, we could not detect SnRK1β1 or SnRK1βγ associated with SnRK1α1ΔKA1-GFP (Figure 1C). Moreover, in the absence of regulatory subunits the amount of SUMO1 conjugates and hMW SnRK1α1 forms was dramatically reduced (Figure 1B-C), indicating that the regulatory subunits contribute significantly to the overall SUMOylation of the SnRK1 complex. Nevertheless, even if reduced, the presence of SnRK1α1 hMW forms and SUMO1 conjugates in SnRK1α1ΔKA1-GFP immunoprecipitates suggests that the interaction with the regulatory subunits is not strictly necessary for SnRK1α1 SUMOylation.

Collectively, these results indicate that several subunits of the SnRK1 complex are SUMOylated *in planta* and that this may involve the formation of SUMO chains and/or the modification of multiple residues.

SUMOylation inhibits SnRK1 signaling and is SIZ1-dependent

To investigate whether SUMOylation has an impact on SnRK1 signaling, we first undertook a mutagenesis approach to block SnRK1 SUMOylation. We focused on the major catalytic subunit SnRK1α1, as it accounts for nearly 90% of SnRK1 activity *in planta* (Jossier *et al.* 2009). SnRK1 harbors two predicted SUMOylation sites [K144 and K471, Figure S4A; (Elrouby and Coupland 2010)], but their mutation to arginine, individually or in combination, did not prevent SUMOylation in the *E. coli* assay (Figure S4B). To map roughly the site(s) of SUMOylation we used the kinase (KD, 1-293) and the regulatory domain (RD, 294-512) (Figure S4A) as substrates in the *E. coli* assay, and found that SnRK1α1 is SUMOylated on both (Figure S4C). To identify the target lysines, we performed Liquid Chromatography-Tandem Mass Spectrometry (LC-MS/MS) analyses employing regular mature SUMO3 (SUMO3-GG) and a variant ($SUMO3^{S91R}$-GG) that facilitates LC-MS/MS analyses by yielding a small tryptic footprint (Okada *et al.* 2009). We focused these analyses on SUMO3 because it generated similar SUMOylation patterns but with stronger signal intensity than SUMO1, allowing a better yield for LC-MS/MS. We uncovered nine SUMOylated lysines (including K144 but not K471), of which two are located in the KA1 domain and seven in the Kinase Domain (Figure S4A and S4D). The structural model of the SnRK1 complex predicts that all of these residues are accessible to solvent (Figure S4D, residues indicated). A single K390R mutation and a double K34R/K63R mutation were sufficient to abrogate SUMOylation of the RD and KD, respectively (Figure S4E). Furthermore, SUMOylation could no longer be detected in the full-length $SnRK1\alpha1^{K34/63/390R}$ triple mutant (hereafter referred as $SnRK1\alpha1^{3K}$, Figure S4F), suggesting that these three lysines are the genuine targets of SUMOylation *in vivo*.

We next assessed the functional relevance of SnRK1 SUMOylation in a cell-based reporter gene assay by comparing SnRK1 activity between SnRK1α1, $SnRK1\alpha1^{3K}$, and a SnRK1α1 variant mutated in all SUMOylated lysines ($SnRK1\alpha1^{K20/34/44/56/63/69/390/421R}$,

hereafter referred as SnRK1α1^{8K}) except K144, as the K144R mutation abolishes kinase activity [(Cho *et al.* 2012)]. In this assay, SnRK1 activity is measured as an induction of the *pDIN6::LUC* reporter and transient SnRK1α1 overexpression is sufficient to trigger strong SnRK1 signaling and reporter activation (Baena-Gonzalez *et al.* 2007; Rodrigues *et al.* 2013). As expected, SnRK1α1 overexpression resulted in 20–fold activation of the *pDIN6::LUC* reporter, whilst an inactive SnRK1α1^{T175A} kinase [T-loop phosphomutant, (Baena-Gonzalez *et al.* 2007)] had no effect. However, the two SnRK1α1^{3K} and SnRK1α1^{8K} variants induced the reporter normally (Figure 2A), suggesting that *in planta* SnRK1α1 can be SUMOylated on other residues and/or that SUMOylation of other components of the complex (*e.g.* the β-regulatory subunits) is sufficient to convey the SUMO signal.

As an alternative strategy to globally block SUMOylation of the SnRK1 complex and to assess its functional relevance, we set to identify the E3 ligase(s) responsible for this modification. Even though SCE1 is sufficient for conjugating the SUMO peptide to a substrate *in vitro*, SUMO E3 ligases are important for substrate specificity and SUMOylation efficiency *in vivo* (Novatchkova *et al.* 2012). In Arabidopsis, only two SUMO E3 ligases have been identified, SIZ1 and HPY2 (Ishida *et al.* 2009; Miura and Hasegawa 2010; Miura *et al.* 2005; Novatchkova *et al.* 2012). Given the strong association of SIZ1 with plant stress responses and the involvement of HPY2/MMS21 mostly in developmental processes (Castro *et al.* 2012), we hypothesized that SnRK1 SUMOylation is mediated by SIZ1. To test this, we introduced the *pSnRK1α1::SnRK1α1-GFP::tSnRK1α1* construct in *siz1-2*, a null mutant of SIZ1 [(Miura *et al.* 2005); hereafter referred as *SnRK1α1-GFP*$_{siz1-2}$] to perform GFP pull-downs and immunoblot analyses as previously described (Figure 1B). As shown in Figure 2B, Western blot analyses of immunoprecipitated SnRK1-GFP revealed a complete absence of SUMO1 conjugates in the *siz1-2* mutant, demonstrating that SIZ1 is responsible for SnRK1 SUMOylation by SUMO1 *in planta.* Importantly, the relative abundance of hMW SnRK1α1

forms in *SnRK1α1-GFP*$_{siz1-2}$ was strongly reduced (more than 50%) when compared to *SnRK1α1-GFP* plants, indicating that a significant part of these forms corresponds to SUMOylated SnRK1α1 (Figure 2B).

Having established SIZ1 as the E3 ligase responsible for SnRK1 SUMOylation, we next investigated the functional relevance of this modification by comparing SnRK1 signaling in Col-0 (wild-type, WT) and *siz1-2* plants. To this end, we treated plants with control (3h light) or SnRK1 signaling activating conditions (3h of darkness during the day) and measured the expression of SnRK1 target genes by quantitative RT-PCR (qRT-PCR) as readout of SnRK1 pathway activation (Baena-Gonzalez *et al.* 2007; Rodrigues *et al.* 2013). As expected, exposure to darkness triggered a strong induction of SnRK1 target genes (*AXP*, *DIN6* and *TPS8*) in Col-0 plants (Figure 2C). This induction was two-fold higher in the *siz1-2* mutant, showing that SIZ1 is a negative regulator of SnRK1 signaling (Figure 2C). Given that the dwarf growth of *siz1-2* is largely caused by elevated salicylic acid (SA) levels (Lee *et al.* 2007; Miura *et al.* 2010), we asked if the effect of the *siz1-2* mutation on SnRK1 signaling was indirect, and induced by SA. To test this, we treated Col-0 protoplasts transfected with the *pDIN6::LUC* reporter and SnRK1α1 or control DNA, with SA or ethanol (mock-treated). As shown in Figure S5A, SA had no effect on SnRK1 signaling during a short (2h) or extended (15h) incubation. Furthermore, examination of public microarray datasets with the Genevestigator tool (Hruz *et al.* 2008) revealed that various SA treatments induce Systemic Acquired Resistance (SAR) marker genes, but not SnRK1 marker genes (*DIN6*, *AXP* and *TPS8*) (Figure S5B), ruling out an indirect effect of the *siz1-2* mutation on SnRK1 signaling through SA. To further evaluate potential pleiotropic effects of the *siz1-2* mutation on SnRK1 signaling, we next compared reporter gene activation by SnRK1α1 in protoplasts from Col-0 and *siz1-2* plants. Expression of SnRK1α1 in Col-0 protoplasts triggered the expected activation of the *pDIN6::LUC* reporter (Figure 2D). However, this activation was 3-fold

higher in the *siz1-2* mutant, consistent with the hyperactivation of endogenous marker genes in response to dark stress (Figure 2C). Most importantly, co-expression of SIZ1 but not of a catalytically inactive SIZ1 variant [$SIZ1^{C379A}$; (Cheong *et al.* 2009)] restored normal activation of the reporter in *siz1-2* (Figure 2D), supporting the lack of activity of this SUMO E3 ligase as the cause for hyperactive SnRK1 signaling in the mutant. We next triggered SnRK1 signaling in an alternative manner, by expressing the GBF5 transcription factor that acts downstream of SnRK1 (Baena-Gonzalez *et al.* 2007). GBF5 induced the expected activation of the *pDIN6::LUC* reporter in Col-0 protoplasts and this activation was similar in the *siz1-2* mutant (Figure 2E), providing additional evidence that repression of SnRK1 signaling by SIZ1 occurs at the level of the SnRK1 kinase.

Altogether, these results show that SIZ1 inhibits SnRK1 signaling, most probably through SUMOylation of several components of the SnRK1 complex.

SUMOylation triggers SnRK1 degradation

Proteins modified by SUMO acquire novel molecular features that can affect their stability, activity, and/or subcellular localization, primarily through altered interactions with other proteins (Jentsch and Psakhye 2013). To determine whether the SIZ1-dependent inhibition of SnRK1 involved changes on SnRK1 specific activity, we performed *in vitro* kinase assays using immunoprecipitated SnRK1α1 and ABF2 as a substrate (Rodrigues *et al.* 2013). Even though ABF2 phosphorylation was two-fold higher with SnRK1 immunoprecipitated from the *siz1-2* mutant than from the Col-0 control, this was fully explained by the two-fold higher levels of SnRK1α1 immunoprecipitated from *siz1-2* plants (Figure 3A). This shows that the over-activation of SnRK1 signaling in *siz1-2* plants is not caused by changes in SnRK1 specific activity, but rather by an enhanced accumulation of the kinase.

To determine more precisely SnRK1 levels, we performed immunoblot analyses using total soluble protein extracts. These analyses confirmed that SnRK1α1 is about 2.5-fold more abundant in the *siz1-2* mutant. As a result of increased accumulation, SnRK1α1 T-loop phosphorylation is also 2.5-fold higher in the *siz1-2* mutant, consistent with a similar SnRK1 specific activity in Col-0 and *siz1-2* plants (Figure 3A). The levels of phosphorylated SnRK1α2 were also higher in *siz1-2*, suggesting this other catalytic subunit might also be a target of SUMOylation. In accordance with our previous indications that SUMOylation could target the regulatory subunits (Figure 1 and 2A), we also detected an increase in SnRK1β1 protein amounts in *siz1-2* (Figure 3C). Similar comparisons were not possible for SnRK1βγ since the available antibodies recognize multiple bands in total protein extracts (Figure S6), despite being adequate for analyzing SnRK1 immunoprecipitates (Figure 1C). Interestingly, SnRK1γ displayed a 3.5-fold accumulation in the *siz1-2* mutant (Figure S2B), although, in accordance with previous reports (Emanuelle *et al.* 2015; Ramon *et al.* 2013), we could not detect this protein in SnRK1α1 immunoprecipitates (Figure S2C).

To investigate the cause of enhanced SnRK1 accumulation in *siz1-2*, we next performed protein half-life measurements in Col-0 and *siz1-2* protoplasts expressing SnRK1α1. Following 6h of incubation, translation was blocked by the addition of cycloheximide (CHX) and cells were harvested after 2 and 4 hours for quantification of SnRK1α1 amounts. As shown in Figure 3D, SnRK1α1 degradation was mostly abolished in the *siz1-2* mutant. To assess whether the lack of SnRK1α1 degradation in *siz1-2* is due to the lack of SUMOylation, we generated a translational fusion between SnRK1α1 and a non-conjugatable mature SUMO1-AA (SnRK1α1-SUMO1), thus mimicking SnRK1α1 SUMOylation [”SUMO mimetic” (Ulrich 2009)]. Interestingly, the SnRK1α1 SUMO mimetic was degraded in *siz1-2* to a similar extent as SnRK1α1 in Col-0 protoplasts (Figure 3D). Moreover, mimicking SUMOylation with the SnRK1α1-SUMO1 variant bypassed SIZ1 and

restored normal *pDIN6::LUC* reporter activation in the *siz1-2* mutant (Figure 3E), altogether supporting the view that SUMOylation of SnRK1α1 promotes its degradation.

SUMOylated SnRK1 is ubiquitinated and degraded by the proteasome

We next asked whether the observed SnRK1 degradation occurred *via* the ubiquitin proteasome system. To assess this, we determined SnRK1α1 accumulation in the presence of the proteasome inhibitor MG132 or the DMSO solvent control. In accordance with previous results (Figure 3D), we observed a strong reduction in SnRK1α1 levels 3h after the addition of cycloheximide (Figure 4A). However, this degradation was significantly blocked in cells treated with MG132, showing that SnRK1α1 protein turnover is largely dependent on the proteasome.

To investigate whether SnRK1 is ubiquitinated for proteasomal degradation *in planta*, we employed the same system as for assessing SnRK1 SUMOylation (Figure 1B) and performed GFP immunoprecipitation from *SnRK1α1-GFP*, *SnRK1α1ΔKA1-GFP*, and *35S::GFP* control plants, to check for the presence of ubiquitin conjugates. These analyses revealed a higher accumulation of ubiquitin conjugates in immunoprecipitates from *SnRK1α1-GFP* than in those from *SnRK1α1ΔKA1-GFP* plants, while none were detected in the *35S::GFP* control (Figure 4B). This pattern was clearly similar to that of SUMO conjugates (Figure 1B), suggesting that SnRK1 ubiquitination and SUMOylation may be interconnected. To test whether SnRK1 SUMOylation is a prerequisite for its ubiquitination, we next immunoprecipitated SnRK1α1-GFP from *SnRK1α1-GFP*$_{siz1-2}$ plants and checked for the presence of ubiquitin. As shown in Figure 4C, ubiquitin conjugates were markedly reduced in SnRK1α1-GFP immunoprecipitates from *SnRK1α1-GFP*$_{siz1-2}$ compared to *SnRK1α1-GFP* plants, indicating that SnRK1 SUMOylation is at least partially required for its subsequent ubiquitination.

343

344 **SnRK1 degradation is strictly dependent on its activity**

345 We previously observed that inactive SnRK1α1 variants, such as SnRK1α1^{T175A} and
346 SnRK1α1^{K48M} (impaired in phosphotransfer activity), accumulate to higher levels than active
347 SnRK1α1 (Baena-Gonzalez *et al.* 2007) (Figure 5A), suggesting a connection between kinase
348 activity and stability. By measuring protein half-life in the presence of cycloheximide in Col-
349 0 cells, we found that the reason for over-accumulation of both inactive variants
350 (SnRK1α1^{K48M} and SnRK1α1^{T175A}) was the lack of protein degradation (Figure 5B).

351 Given the enhanced stability of SnRK1α1 in the *siz1-2* mutant (Figure 3C), we next
352 asked whether the increased stability of the inactive SnRK1α1 variants could also be due to a
353 lack of SUMOylation. To test this, we generated SUMO-mimetics of all three SnRK1α1
354 variants and measured their half-life. Degradation of active SnRK1α1 did not seem to be
355 altered in the corresponding SUMO-mimetic (Figures 3D and 5C), suggesting that
356 SUMOylation might not be rate-limiting for degradation of the active kinase. However, the
357 SUMO-mimetic forms of the inactive variants were readily degraded, displaying the same
358 degradation profile as active SnRK1α1. In contrast, a SUMO mimetic of a GFP control
359 protein was stable over time, demonstrating a specific effect of SUMO on SnRK1α1 stability.

360 Collectively, these results confirm the link between SnRK1 activity and turnover and
361 indicate that SUMOylation is an intermediary step in this process.

362

363 **DISCUSSION**

364 Deregulation of kinase activity often results in cellular or whole-organism dysfunction and
365 even lethality (Lu and Hunter 2009). Indeed, in yeast, inappropriately high SNF1 activity is
366 deleterious to cell growth, as mutants of the inhibitory phosphatases are only viable if
367 expressing a SNF1 variant with reduced catalytic activity (Ruiz *et al.* 2011; Ruiz *et al.* 2013).

On the other hand, sugar provision stimulates growth in WT seedlings but not in plants overexpressing SnRK1α1, presumably due to excessive repression of biosynthetic activities when SnRK1 is hyperactive (Baena-Gonzalez *et al.* 2007). Being a key regulator of the stress response, growth and development, SnRK1 activity must hence be counterbalanced by mechanisms that restrain its action. In this study, we provide strong evidence suggesting that SUMOylation is such a mechanism (Figure 6). SnRK1 is SUMOylated by the SIZ1 E3 SUMO ligase, resulting in its ubiquitination and proteasomal degradation. Mutations that abolish kinase activity prevent SnRK1 degradation, suggesting that SnRK1 activity and SUMOylation are tightly coupled in a negative feedback loop to prevent detrimental pathway hyperactivation.

An increasing number of studies show that SUMO E3 ligases often act on preassembled protein complexes, modifying groups of physically interacting components rather than individual proteins (Jentsch and Psakhye 2013). In agreement with this, our results indicate that SUMOylation occurs at the level of the whole SnRK1 complex (Figure 1, 3, and S2A) and that SIZ1 is responsible for this modification (Figure 2B). The view of collective SnRK1 SUMOylation is further supported by our inability to alter SnRK1 function by mutating the target lysines of the SnRK1α1 subunit (Figures S4F and 2A), as presumably SUMOylation of the remaining subunits compensates for the lack of SUMOylation in SnRK1α1. A "SUMOylation wave" targeting several members of a protein complex has been described, amongst others, for the DNA damage repair complex, in which mutation of single subunits is not sufficient to abrogate SUMOylation of the complex and to cause functional defects (Jentsch and Psakhye 2013).

Our functional analyses revealed that the SnRK1 pathway is hyperactivated in the *siz1-2* mutant, and that the SnRK1 kinase is repressed by SIZ1 (Figure 2C-D). Although we cannot currently rule out the contribution of other proteins to the overactivation of energy

signaling in the *siz1-2* mutant, the fact that the downstream transcription factor GBF5 induces normal activation of the pathway in *siz1-2* cells (Figure 2E) supports the hypothesis that the defect is mainly at the SnRK1 level.

Importantly, normal activation of the SnRK1 pathway in *siz1-2* could be restored by transient complementation with SIZ1 but not with a catalytically inactive $SIZ1^{C379A}$ variant (Figure 2D), underscoring the importance of this ligase activity for SnRK1 regulation and ruling out long-term pleiotropic effects of the *siz1-2* mutation on SnRK1 function. We could further show that the cause of SnRK1 pathway hyperactivation in the *siz1-2* mutant was an increased SnRK1 accumulation (Figure 3A-C and S2C). Interestingly, the increase in protein amounts was not stoichiometric, as SnRK1β1 accumulation in *siz1-2* exceeded nearly six-fold that of the SnRK1α1 subunit. This is probably because, in addition to the effect of SIZ1 on SnRK1 protein accumulation, the *SnRK1β1* gene is strongly induced by SnRK1 signaling (Baena-Gonzalez *et al.* 2007), which is higher in *siz1-2* (Figure 2)

Protein half-life measurements, using SnRK1α1 as a representative of the SnRK1 complex, revealed that the reason for enhanced SnRK1 accumulation in *siz1-2* cells was a defect in protein degradation (Figure 3D). Moreover, mimicking SnRK1α1 SUMOylation was sufficient to rescue its degradation (Figure 3D) and normal pathway activation (Figure 3E) in the *siz1-2* mutant, indicating that the cause of impaired SnRK1α1 degradation is the lack of SUMOylation. SnRK1 seems to be degraded by the 26S proteasome, as it is strongly ubiquitinated (Figure 4B) and its degradation is largely blocked by MG132 (Figure 4A). This is consistent with high-throughput analyses in which SnRK1α1 was identified as a target for ubiquitination and was stabilized by MG132 (Kim *et al.* 2013; Maor *et al.* 2007). On the other hand, SnRK1 ubiquitination is largely dependent on SUMOylation, as the presence of ubiquitin conjugates in SnRK1α1 immunoprecipitates was greatly reduced in the *siz1-2* mutant (Figure 4C). How SUMOylated SnRK1 is targeted to proteasomal degradation is

currently unknown but the process is likely to involve the action of the recently discovered E4 SUMO ligases, responsible for (poly)SUMO chain formation (Tomanov *et al.* 2014), and/or the SUMO-targeted Ubiquitin Ligases (StUbLs), responsible for the ubiquitination of SUMOylated substrates (Elrouby *et al.* 2013).

Protein kinases are often targeted by more than one E3 ubiquitin ligases, with some E3 ligases acting specifically on the active kinase (Lu and Hunter 2009). The fact that in the *siz1-2* mutant we could still detect hMW SnRK1α1 forms (Figure 2B) as well as SnRK1α1-associated ubiquitin conjugates (Figure 4C), supports the existence of parallel SUMO-independent ubiquitination pathways. SnRK1α1 interacts with Pleiotropic Regulatory Locus 1 (PRL1) (Bhalerao *et al.* 1999) and SnRK1α1 degradation is mediated by the DDB1-CUL4-ROC1-PRL1 E3 ubiquitin ligase, in which PRL1 is the putative substrate receptor of the complex (Lee *et al.* 2008). Proteasomal degradation of SnRK1α1 was also shown to occur in a Myoinositol Polyphosphate 5-Phosphatase 13 (5PTase13)-dependent manner (Ananieva *et al.* 2008). Whether PRL1, 5PTase13, and SIZ1 act in same pathway or in parallel ones is currently unknown.

We show here that SUMO-mediated degradation of SnRK1 is strictly dependent on SnRK1 kinase activity. Inactive SnRK1α1 variants are not degraded (Figure 5B), accumulating to much higher levels than the active kinase (Baena-Gonzalez *et al.* 2007) (Figure 5A). The reason for the increased stability of the inactive SnRK1α1 variants appears to be the lack of SUMOylation, as they recover normal turnover when expressed as SUMO mimetics (Figure 5D). Activated kinases can be recognized for ubiquitination and degradation by different mechanisms, often involving the generation of recognition motifs through phosphorylation or the exposure of such motifs through conformational changes (Lu and Hunter 2009). An intriguing question that remains open is how the SUMO machinery recognizes active SnRK1.

SUMOylation has also been described for AMPK and SNF1, affecting these kinases in various ways. In AMPK, both catalytic (α1/α2) subunits are within a list of ~1600 human proteins found to be SUMOylated using high-resolution MS (Hendriks *et al.* 2014). AMPKα1 SUMOylation was detected in control samples and was significantly increased in response to SUMO protease inhibition, proteasome inhibition and heat shock treatments, suggesting that, likewise SnRK1 SUMOylation, it might also be involved in signal termination. Interestingly, the lysine identified by Hendriks and colleagues corresponds to K390 in SnRK1α1, also found SUMOylated in our study (Figure S4). Another recent report showed that also AMPKβ2 is SUMOylated (Rubio *et al.* 2013). However, SUMOylation of AMPKβ2 did not affect its degradation rate but instead enhanced AMPK activity by increasing T-loop phosphorylation. Furthermore, AMPKβ2 SUMOylation and ubiquitination appeared to be antagonistic rather than interdependent processes. In the case of SNF1, the Snf1 catalytic subunit was reported to be SUMOylated in response to glucose and to downregulate SNF1 independently of T-loop phosphorylation in two ways (Simpson-Lavy and Johnston 2013). Firstly, SUMOylation of Snf1 caused a rapid inhibition of the kinase specific activity, presumably *via* a conformational switch induced by the interaction between the SUMOylated residue and a SUMO-interacting motif (SIM). It is unlikely that such a mechanism is conserved as the target lysine (K549) implicated in this regulation is not conserved (Figure S7B). However, the possibility that the conserved SIM1 (Figure S7A, T89-V94 in SnRK1α1) plays a role in SnRK1 SUMOylation remains to be established. Furthermore, whilst SNF1 is SUMOylated on a single residue on the catalytic subunit, SnRK1 seems to be SUMOylated on multiple residues/subunits. Secondly, SUMOylation of Snf1 upon glucose feeding induced its degradation, from which the authors concluded that SUMOylation is important to reduce SNF1 levels when cells do no longer need SNF1 activity. Nevertheless, the fact that the Mms21 SUMO (E3) ligase mutant accumulates higher Snf1 levels under low glucose

conditions (Simpson-Lavy and Johnston 2013) suggests that, likewise SnRK1 and AMPK, SNF1 SUMOylation may also prevent pathway hyperactivation when SNF1 is active.

In summary, our work has uncovered a negative feedback loop by which SnRK1 activity triggers its own SUMO-mediated proteasomal degradation. We postulate that this intimate connection between kinase activity and accumulation is evolutionarily conserved and that it may be essential for balancing stress and defense responses with biosynthetic activities, cell proliferation, and growth (Baena-Gonzalez and Sheen 2008; Huot *et al.* 2014).

EXPERIMENTAL PROCEDURES

Primers and Constructs

A list of all primers, cloning steps, and constructs used in this study is provided in Table S1.

Plant Material and Growth Conditions

Unless otherwise specified, plants were grown in soil under a 12h light (100µE), 22°C/12h dark, 18°C regime. All *Arabidopsis thaliana* plants used in this study are in the Columbia (Col-0) background. The *siz1-2* (Miura *et al.* 2005) and *35S::SnRK1α1* [(Jossier *et al.* 2009), *35S::SnRK1.1-2*] plants have been previously described. The generation of *35S::GFP, SnRK1α1-GFP*, *SnRK1α1ΔKA1-GFP and* $SnRK1\alpha1\text{-}GFP_{siz1\text{-}2}$ lines is fully described in Methods S1.

GFP, SnRK1α1-GFP and SnRK1α1ΔKA1-GFP Immunoprecipitation

Proteins from 5-week-old *SnRK1α1-GFP*, *SnRK1α1ΔKA1-GFP,* $SnRK1\alpha1\text{-}GFP_{siz1\text{-}2}$ or *35S::GFP* plant leaves were extracted with immunoprecipitation (IP) buffer [50mM Tris-HCl pH8.0, 50mM NaCl, 1% (V/V) Igepal CA-630, 0.5% (w/V) Sodium deoxycholate, 0.1%

(w/V) SDS, 1mM EDTA pH8.0, 50µM MG132, 50mM *N*-Ethylmaleimide and cOmplete protease inhibitor cocktail (one tablet/10mL)]. After clearing samples by centrifugation (6,785g, 2°C, 10min) 800µL of supernatant were supplemented with fresh MG132 (50µM) and incubated at 4°C for 1h with 40µL of µMACS Anti-GFP MicroBeads (µMACS GFP Isolation Kit, Miltenyi, 130-091-125). Samples were thereafter loaded in µColumns (Miltenyi, 130-042-701) pre-equilibrated with 1ml of IP buffer, and allowed to flow through. Columns were washed three times with 200µL and once with 600µL of IP buffer and proteins eluted with 80µL of Elution Buffer (Miltenyi, 130-091-125) at 95°C. β-Mercapto-Ethanol (2%) was added to the eluates prior to boiling for 5 min at 95°C. Proteins were resolved by SDS-PAGE, wet-transferred to a PVDF membrane (30V, 16h at 4°C), and analyzed by immunoblotting with SnRK1α1, SnRK1β1, SnRK1γ, SnRK1βγ, SUMO1, UBQ11 and GFP antibodies. For each GFP immunoprecipitation experiment, immunodetection with different antibodies was done using equal loading on independent membranes.

SnRK1α1 Immunoprecipitation and *in Vitro* Kinase Assays

For measurements of endogenous SnRK1α1 activity, SnRK1α1 was immunoprecipitated from leaves of 5-week-old Col-0 or *siz1-2* plants. Plant material (1g) was extracted in 2 volumes of Buffer C [50mM Hepes, pH7.25, 150mM NaCl, 1mM EDTA, 0.05% Triton X-100, cOmplete protease inhibitor cocktail (one tablet/50mL, Roche 11697498001) and 1/500 (v/v) phosphatase inhibitor 2 (Sigma P5726) and 3 (Sigma P0044)]. After two successive centrifugations (20,000g, 4°C, 10min), the supernatant was recovered and filtered (0.45µm) and 1 mg of total protein (quantified using the Bradford protein assay) was incubated with gentle shaking for 3h at 4°C with 15µL beads of protein A–antibody complex prepared as follows. For each immunoprecipitation, 15µL (bed volume) of protein A–agarose (Roche #11719408001) was equilibrated in 1XPBS (Sigma-Aldrich P5493) and incubated with 1.5µg

of anti-SnRK1α1 antibody (anti-AKIN10) in 500µL of 1X PBS for 1h at room temperature with gentle shaking. After three washes in buffer C, the beads were used for immunoprecipitation. After incubation for 3h at 4°C under shaking, the beads were washed five times with buffer C, and one-third (5µL) was kept for immunoblot analyses with an anti-SnRK1α1 antibody. The remaining 10µL were used to determine the specific activity of SnRK1 in 30µL of kinase buffer (50mM Hepes-NaOH, pH7.25, 20mM $MgCl_2$, 0.5mM DTT and 100mM ATP) with His-ΔC ABF2 (1µg) for 1 h at 30°C in the presence of 2µCi of γ^{32}P-ATP. The reaction products were resolved by 12% SDS-PAGE and detected using a phosphor image system (STORM 860, GE Healthcare).

Antibodies and Western-blotting

The SnRK1α1 (1/500, anti-AKIN10, AS10919), SnRK1β1 (1/500, anti-AKINB1, AS09460), SnRK1βγ (1/1000, anti-AKINBG, AS09463, Figure S6) and SnRK1γ (1/2000, anti-AKING1, AS09613) were purchased from Agrisera. Phospho-SnRK1α1/2 (T175/176) was detected with an anti–phosphoT172-AMPKα antibody (1/1000 in 5% BSA-TBS-Tween, referred to as P-AMPK; #2535, Cell Signaling). SUMO1 (1/5000, ab5316, Abcam) and Ubiquitin11 (1/10000, AS08307, Agrisera) antibodies were used to detect the respective protein modifications. Anti-HA (1/1000, Roche, #11867423001), anti-GFP (1/1000, 11814460001, Roche) and anti-T7 (1/10000, #69522-3, Novagen) antibodies were used to detect the corresponding tagged proteins.

For immunoblotting all primary antibodies were diluted in 1% non-fat Milk in TBS (unless otherwise stated) and incubated with the membrane under gentle shaking for 12h at 4°C. Secondary antibodies (Jackson ImmunoResearch Lab, inc) were used at 1/10000 in 1% non-fat Milk in TBS for 1h at RT. In the case of immunoprecipitated samples, secondary antibodies subsequently used in the immunodetection were against the light chain of IgG.

Protoplast Transient Expression Assays

Protoplasts from Col-0 and *siz1-2* plants were isolated and transfected as already described (Yoo *et al.* 2007). All effector constructs (Table S1) were generated by cloning the corresponding coding sequences into a pHBT95 vector harboring a C-terminal HA or GFP tag (Yoo *et al.* 2007), except for C-terminal fusions with mSUMO1AA, for which the GFP/HA tag was replaced with mSUMO1AA. The indicated mutations were introduced by site-directed mutagenesis and verified by sequencing. SnRK1 signaling was monitored using a *pDIN6::LUC* reporter, and the *pUBQ10::β-glucuronidase* reporter as transfection efficiency control (Baena-Gonzalez *et al.* 2007). For SA treatment, transfected protoplasts were incubated for 4h to allow protein expression and were thereafter treated with SA (5µM) or ethanol (mock) for 2h or overnight. For analyses of protein degradation proteins were expressed for 6h, CHX (100µM) and/or MG132 (50µM) were added, and cells were thereafter harvested at the indicated time points. Frozen cell pellets were resuspended in 4X Laemmli solubilization buffer, boiled for 5min at 95°C and analyzed by Western blot.

Gene Expression Analyses

Fully expanded rosettes of 4-5-week-old Col-0 and *siz1-2* plants were incubated on sterile MilliQ water in Petri dishes under control (3h Light, 100µE) or SnRK1 signaling activating conditions (3h Dark). The treatment was always initiated 3h after the onset of the light period. Total RNA was extracted using TRIzol reagent (Life Technologies), treated with RNase-Free DNase (Promega), and reverse transcribed (1µg) using SuperScript III Reverse Transcriptase (Life Technologies), as previously described (Rodrigues *et al.* 2013). Quantitative real-time RT-PCR (qPCR) analyses were performed using a CFX384TM Real-Time System (Bio-Rad), the iTaqTM Universal SYBR® Green Supermix (BioRad), and the $2^{-\Delta\Delta Ct}$ method for relative

quantification (Livak and Schmittgen 2001). Expression values of SnRK1 target genes were normalized using the CT values obtained for the *ACT2* reference gene.

ACCESSION NUMBERS

Sequence data from this article can be found in the Arabidopsis Genome Initiative database under the following accession numbers: *SnRK1α1*, At3g01090; *SnRK1α2*, At3g29160; *SnRK1β1*, At5g21170; *SnRK1β2*, At4g16360; *SnRK1γ*, At3g48530; *SnRK1βγ*, At1g09020; *GBF5*, At2g18160; *SIZ1*, At5g60410; *HPY2*, At3g15150; *SUMO1*, At4g26840; *SUMO3*, At5g55170; *SCE1*, At3g57870; *DIN6*, At3g47340; *AXP*, At2g33830; *TPS8*, At1g70290; *ACT2*, At3g18780; *UBQ10*, At4g05320.

ACKNOWLEDGEMENTS

We thank Vera Nunes for excellent plant management and K. Miura, K. Tanaka, and M. Thomas for kindly providing the *siz1-2* mutant, the plasmids for the *E. coli* SUMOylation assay, and the constructs for expression of recombinant SnRK1 subunits, respectively. This work was supported by the Austrian Science Foundation FWF (grant P25488 to AB and P23435 to MT); the EMBO Installation program (to EBG) and grant PTDC/BIA-PLA/3937/2012 (to EBG), UID/Multi/04551/2013_Research unit GREEN-it_"Bioresources for Sustainability" (to EBG), SFRH/BD/51627/2011 (to LM), SFRH/BPD/79255/2011 (to PC) from Fundação para a Ciência e a Tecnologia. The authors declare no conflict of interest.

SUPPORTING INFORMATION

Additional Supporting Information may be found in the online version of this article.

Figure S1. SnRK1α1 interacts with the SUMO E2 Conjugating Enzyme 1 (SCE1) in a Yeast two-Hybrid assay

Figure S2. SnRK1γ is SUMOylated in *E. coli* and enriched in *siz1-2*, but is not part of the SnRK1α1 complex in Arabidopsis leaves

Figure S3. Generation of *SnRK1α1-GFP* transgenic lines

Figure S4. SnRK1α1 residues found SUMOylated in the *E. coli* assay

Figure S5. Salicylic acid (SA) has no effect on SnRK1 signaling

Figure S6. Specificity of the anti-SnRK1βγ antibody

Figure S7. Conservation in SnRK1α1 of the residues implicated in SNF1 SUMOylation

Table S1. List of primers used in this study

Methods S1

REFERENCES

Ananieva, E.A., Gillaspy, G.E., Ely, A., Burnette, R.N. and Erickson, F.L. (2008) Interaction of the WD40 Domain of a Myoinositol Polyphosphate 5-Phosphatase with SnRK1 Links Inositol, Sugar, and Stress Signaling. *Plant Physiol*, **148**, 1868-1882.

Baena-Gonzalez, E., Rolland, F., Thevelein, J.M. and Sheen, J. (2007) A central integrator of transcription networks in plant stress and energy signalling. *Nature*, **448**, 938-942.

Baena-Gonzalez, E. and Sheen, J. (2008) Convergent energy and stress signaling. *Trends Plant Sci*, **13**, 474-482.

Bhalerao, R.P., Salchert, K., Bako, L., Okresz, L., Szabados, L., Muranaka, T., Machida, Y., Schell, J. and Koncz, C. (1999) Regulatory interaction of PRL1 WD protein with Arabidopsis SNF1-like protein kinases. *Proc Natl Acad Sci U S A*, **96**, 5322-5327.

Castro, P.H., Tavares, R.M., Bejarano, E.R. and Azevedo, H. (2012) SUMO, a heavyweight player in plant abiotic stress responses. *Cell Mol Life Sci*, **69**, 3269-3283.

Cheong, M.S., Park, H.C., Hong, M.J., Lee, J., Choi, W., Jin, J.B., Bohnert, H.J., Lee, S.Y., Bressan, R.A. and Yun, D.J. (2009) Specific domain structures control abscisic acid-, salicylic acid-, and stress-mediated SIZ1 phenotypes. *Plant Physiol*, **151**, 1930-1942.

Cho, Y.H., Hong, J.W., Kim, E.C. and Yoo, S.D. (2012) Regulatory functions of SnRK1 in stress-responsive gene expression and in plant growth and development. *Plant Physiol*, **158**, 1955-1964.

Coello, P., Hirano, E., Hey, S.J., Muttucumaru, N., Martinez-Barajas, E., Parry, M.A. and Halford, N.G. (2012) Evidence that abscisic acid promotes degradation of SNF1-related protein kinase (SnRK1) in wheat and activation of a putative calcium-dependent SnRK2. *J Exp Bot*, **63**, 913-924.

Crozet, P., Margalha, L., Confraria, A., Rodrigues, A., Martinho, C., Adamo, M., Elias, C.A. and Baena-Gonzalez, E. (2014) Mechanisms of regulation of SNF1/AMPK/SnRK1 protein kinases. *Front Plant Sci*, **5**, 190.

Elrouby, N., Bonequi, M.V., Porri, A. and Coupland, G. (2013) Identification of Arabidopsis SUMO-interacting proteins that regulate chromatin activity and developmental transitions. *Proc Natl Acad Sci U S A*, **110**, 19956-19961.

Elrouby, N. and Coupland, G. (2010) Proteome-wide screens for small ubiquitin-like modifier (SUMO) substrates identify Arabidopsis proteins implicated in diverse biological processes. *Proc Natl Acad Sci U S A*, **107**, 17415-17420.

Emanuelle, S., Hossain, M.I., Moller, I.E., Pedersen, H.L., van de Meene, A.M., Doblin, M.S., Koay, A., Oakhill, J.S., Scott, J.W., Willats, W.G., Kemp, B.E., Bacic, A., Gooley, P.R. and Stapleton, D.I. (2015) SnRK1 from Arabidopsis thaliana is an atypical AMPK. *Plant J*, **82**, 183-192.

Fragoso, S., Espindola, L., Paez-Valencia, J., Gamboa, A., Camacho, Y., Martinez-Barajas, E. and Coello, P. (2009) SnRK1 isoforms AKIN10 and AKIN11 are differentially regulated in Arabidopsis plants under phosphate starvation. *Plant Physiol*, **149**, 1906-1916.

Geiss-Friedlander, R. and Melchior, F. (2007) Concepts in sumoylation: a decade on. *Nat Rev Mol Cell Biol*, **8**, 947-956.

Guo, C. and Henley, J.M. (2014) Wrestling with stress: Roles of protein SUMOylation and deSUMOylation in cell stress response. *IUBMB Life*, **66**, 71-77.

Hao, L., Wang, H., Sunter, G. and Bisaro, D.M. (2003) Geminivirus AL2 and L2 proteins interact with and inactivate SNF1 kinase. *Plant Cell*, **15**, 1034-1048.

Hendriks, I.A., D'Souza, R.C., Yang, B., Verlaan-de Vries, M., Mann, M. and Vertegaal, A.C. (2014) Uncovering global SUMOylation signaling networks in a site-specific manner. *Nat Struct Mol Biol*, **21**, 927-936.

Hruz, T., Laule, O., Szabo, G., Wessendorp, F., Bleuler, S., Oertle, L., Widmayer, P., Gruissem, W. and Zimmermann, P. (2008) Genevestigator v3: a reference expression database for the meta-analysis of transcriptomes. *Adv Bioinformatics*, **2008**, 420747.

Huot, B., Yao, J., Montgomery, B.L. and He, S.Y. (2014) Growth-defense tradeoffs in plants: a balancing act to optimize fitness. *Mol Plant*, **7**, 1267-1287.

Ishida, T., Fujiwara, S., Miura, K., Stacey, N., Yoshimura, M., Schneider, K., Adachi, S., Minamisawa, K., Umeda, M. and Sugimoto, K. (2009) SUMO E3 ligase HIGH PLOIDY2 regulates endocycle onset and meristem maintenance in Arabidopsis. *Plant Cell*, **21**, 2284-2297.

Jentsch, S. and Psakhye, I. (2013) Control of Nuclear Activities by Substrate-Selective and Protein-Group SUMOylation. *Annu Rev Genet*, **47**, 167-186.

Jossier, M., Bouly, J.P., Meimoun, P., Arjmand, A., Lessard, P., Hawley, S., Grahame Hardie, D. and Thomas, M. (2009) SnRK1 (SNF1-related kinase 1) has a central role in sugar and ABA signalling in Arabidopsis thaliana. *Plant J*, **59**, 316-328.

Kim, D.-Y., Scalf, M., Smith, L.M. and Vierstra, R.D. (2013) Advanced Proteomic Analyses Yield a Deep Catalog of Ubiquitylation Targets in Arabidopsis. *The Plant Cell Online*, **25**, 1523-1540.

Kleinow, T., Bhalerao, R., Breuer, F., Umeda, M., Salchert, K. and Koncz, C. (2000) Functional identification of an Arabidopsis snf4 ortholog by screening for heterologous multicopy suppressors of snf4 deficiency in yeast. *Plant J*, **23**, 115-122.

Lastdrager, J., Hanson, J. and Smeekens, S. (2014) Sugar signals and the control of plant growth and development. *J Exp Bot*, **65**, 799-807.

Lee, J., Nam, J., Park, H.C., Na, G., Miura, K., Jin, J.B., Yoo, C.Y., Baek, D., Kim, D.H., Jeong, J.C., Kim, D., Lee, S.Y., Salt, D.E., Mengiste, T., Gong, Q., Ma, S., Bohnert, H.J., Kwak, S.S., Bressan, R.A., Hasegawa, P.M. and Yun, D.J. (2007)

680 Salicylic acid-mediated innate immunity in Arabidopsis is regulated by SIZ1 SUMO
681 E3 ligase. *Plant J*, **49**, 79-90.
682 **Lee, J.H., Terzaghi, W., Gusmaroli, G., Charron, J.B., Yoon, H.J., Chen, H., He, Y.J.,**
683 **Xiong, Y. and Deng, X.W.** (2008) Characterization of Arabidopsis and rice DWD
684 proteins and their roles as substrate receptors for CUL4-RING E3 ubiquitin ligases.
685 *Plant Cell*, **20**, 152-167.
686 **Lee, K.W., Chen, P.W., Lu, C.A., Chen, S., Ho, T.H. and Yu, S.M.** (2009) Coordinated
687 responses to oxygen and sugar deficiency allow rice seedlings to tolerate flooding. *Sci*
688 *Signal*, **2**, ra61.
689 **Lin, C.R., Lee, K.W., Chen, C.Y., Hong, Y.F., Chen, J.L., Lu, C.A., Chen, K.T., Ho, T.H.**
690 **and Yu, S.M.** (2014) SnRK1A-interacting negative regulators modulate the nutrient
691 starvation signaling sensor SnRK1 in source-sink communication in cereal seedlings
692 under abiotic stress. *Plant Cell*, **26**, 808-827.
693 **Livak, K.J. and Schmittgen, T.D.** (2001) Analysis of relative gene expression data using
694 real-time quantitative PCR and the 2(-Delta Delta C(T)) Method. *Methods*, **25**, 402-
695 408.
696 **Lovas, A., Bimbo, A., Szabo, L. and Banfalvi, Z.** (2003) Antisense repression of
697 StubGAL83 affects root and tuber development in potato. *Plant J*, **33**, 139-147.
698 **Lu, C.A., Lin, C.C., Lee, K.W., Chen, J.L., Huang, L.F., Ho, S.L., Liu, H.J., Hsing, Y.I.**
699 **and Yu, S.M.** (2007) The SnRK1A protein kinase plays a key role in sugar signaling
700 during germination and seedling growth of rice. *Plant Cell*, **19**, 2484-2499.
701 **Lu, Z. and Hunter, T.** (2009) Degradation of activated protein kinases by ubiquitination.
702 *Annu Rev Biochem*, **78**, 435-475.
703 **Maor, R., Jones, A., Nühse, T.S., Studholme, D.J., Peck, S.C. and Shirasu, K.** (2007)
704 Multidimensional Protein Identification Technology (MudPIT) Analysis of
705 Ubiquitinated Proteins in Plants. *Molecular & Cellular Proteomics*, **6**, 601-610.
706 **Miller, M.J., Barrett-Wilt, G.A., Hua, Z. and Vierstra, R.D.** (2010) Proteomic analyses
707 identify a diverse array of nuclear processes affected by small ubiquitin-like modifier
708 conjugation in Arabidopsis. *Proc Natl Acad Sci U S A*, **107**, 16512-16517.
709 **Miura, K. and Hasegawa, P.M.** (2010) Sumoylation and other ubiquitin-like post-
710 translational modifications in plants. *Trends in Cell Biology*, **20**, 223-232.
711 **Miura, K., Lee, J., Miura, T. and Hasegawa, P.M.** (2010) SIZ1 controls cell growth and
712 plant development in Arabidopsis through salicylic acid. *Plant Cell Physiol*, **51**, 103-
713 113.
714 **Miura, K., Rus, A., Sharkhuu, A., Yokoi, S., Karthikeyan, A.S., Raghothama, K.G.,**
715 **Baek, D., Koo, Y.D., Jin, J.B., Bressan, R.A., Yun, D.J. and Hasegawa, P.M.**
716 (2005) The Arabidopsis SUMO E3 ligase SIZ1 controls phosphate deficiency
717 responses. *Proc Natl Acad Sci U S A*, **102**, 7760-7765.
718 **Novatchkova, M., Tomanov, K., Hofmann, K., Stuible, H.P. and Bachmair, A.** (2012)
719 Update on sumoylation: defining core components of the plant SUMO conjugation
720 system by phylogenetic comparison. *New Phytol*, **195**, 23-31.
721 **Okada, S., Nagabuchi, M., Takamura, Y., Nakagawa, T., Shinmyozu, K., Nakayama, J.**
722 **and Tanaka, K.** (2009) Reconstitution of Arabidopsis thaliana SUMO pathways in E.
723 coli: functional evaluation of SUMO machinery proteins and mapping of
724 SUMOylation sites by mass spectrometry. *Plant Cell Physiol*, **50**, 1049-1061.
725 **Park, H.J., Kim, W.Y., Park, H.C., Lee, S.Y., Bohnert, H.J. and Yun, D.J.** (2011) SUMO
726 and SUMOylation in plants. *Mol Cells*, **32**, 305-316.
727 **Polge, C., Jossier, M., Crozet, P., Gissot, L. and Thomas, M.** (2008) Beta-subunits of the
728 SnRK1 complexes share a common ancestral function together with expression and

function specificities; physical interaction with nitrate reductase specifically occurs via AKINbeta1-subunit. *Plant Physiol*, **148**, 1570-1582.

Polge, C. and Thomas, M. (2007) SNF1/AMPK/SnRK1 kinases, global regulators at the heart of energy control? *Trends Plant Sci*, **12**, 20-28.

Praefcke, G.J., Hofmann, K. and Dohmen, R.J. (2012) SUMO playing tag with ubiquitin. *Trends Biochem Sci*, **37**, 23-31.

Radchuk, R., Emery, R.J., Weier, D., Vigeolas, H., Geigenberger, P., Lunn, J.E., Feil, R., Weschke, W. and Weber, H. (2010) Sucrose non-fermenting kinase 1 (SnRK1) coordinates metabolic and hormonal signals during pea cotyledon growth and differentiation. *Plant J*, **61**, 324-338.

Radchuk, R., Radchuk, V., Weschke, W., Borisjuk, L. and Weber, H. (2006) Repressing the expression of the SUCROSE NONFERMENTING-1-RELATED PROTEIN KINASE gene in pea embryo causes pleiotropic defects of maturation similar to an abscisic acid-insensitive phenotype. *Plant Physiol*, **140**, 263-278.

Ramon, M., Ruelens, P., Li, Y., Sheen, J., Geuten, K. and Rolland, F. (2013) The hybrid Four-CBS-Domain KINbetagamma-subunit functions as the canonical gamma~subunit of the plant energy sensor SnRK1. *Plant J*, **75**, 11-25.

Rodrigues, A., Adamo, M., Crozet, P., Margalha, L., Confraria, A., Martinho, C., Elias, A., Rabissi, A., Lumbreras, V., Gonzalez-Guzman, M., Antoni, R., Rodriguez, P.L. and Baena-Gonzalez, E. (2013) ABI1 and PP2CA Phosphatases Are Negative Regulators of Snf1-Related Protein Kinase1 Signaling in Arabidopsis. *Plant Cell*, **25**, 3871-3884.

Rubio, T., Vernia, S. and Sanz, P. (2013) Sumoylation of AMPKβ2 subunit enhances AMP-activated protein kinase activity. *Molecular Biology of the Cell*, **24**, 1801-1811.

Ruiz, A., Xu, X. and Carlson, M. (2011) Roles of two protein phosphatases, Reg1-Glc7 and Sit4, and glycogen synthesis in regulation of SNF1 protein kinase. *Proc Natl Acad Sci U S A*, **108**, 6349-6354.

Ruiz, A., Xu, X. and Carlson, M. (2013) Ptc1 protein phosphatase 2C contributes to glucose regulation of SNF1/AMP-activated protein kinase (AMPK) in Saccharomyces cerevisiae. *J Biol Chem*, **288**, 31052-31058.

Saracco, S.A., Miller, M.J., Kurepa, J. and Vierstra, R.D. (2007) Genetic analysis of SUMOylation in Arabidopsis: conjugation of SUMO1 and SUMO2 to nuclear proteins is essential. *Plant Physiol*, **145**, 119-134.

Schwachtje, J., Minchin, P.E., Jahnke, S., van Dongen, J.T., Schittko, U. and Baldwin, I.T. (2006) SNF1-related kinases allow plants to tolerate herbivory by allocating carbon to roots. *Proc Natl Acad Sci U S A*, **103**, 12935-12940.

Simpson-Lavy, K.J. and Johnston, M. (2013) SUMOylation regulates the SNF1 protein kinase. *Proc Natl Acad Sci U S A*, **110**, 17432-17437.

Sugden, C., Donaghy, P.G., Halford, N.G. and Hardie, D.G. (1999) Two SNF1-related protein kinases from spinach leaf phosphorylate and inactivate 3-hydroxy-3-methylglutaryl-coenzyme A reductase, nitrate reductase, and sucrose phosphate synthase in vitro. *Plant Physiol.*, **120**, 257-274.

Thelander, M., Olsson, T. and Ronne, H. (2004) Snf1-related protein kinase 1 is needed for growth in a normal day-night light cycle. *EMBO J*, **23**, 1900-1910.

Tomanov, K., Zeschmann, A., Hermkes, R., Eifler, K., Ziba, I., Grieco, M., Novatchkova, M., Hofmann, K., Hesse, H. and Bachmair, A. (2014) Arabidopsis PIAL1 and 2 Promote SUMO Chain Formation as E4-Type SUMO Ligases and Are Involved in Stress Responses and Sulfur Metabolism. *Plant Cell*, **26**, 4547-4560.

Tsai, A.Y. and Gazzarrini, S. (2012) AKIN10 and FUSCA3 interact to control lateral organ development and phase transitions in Arabidopsis. *Plant J*, **69**, 809-821.

779 **Ulrich, H.D.** (2008) The fast-growing business of SUMO chains. *Mol Cell*, **32**, 301-305.
780 **Ulrich, H.D.** (2009) *SUMO Protocols* New York: Humana Press.
781 **Yoo, S.D., Cho, Y.H. and Sheen, J.** (2007) Arabidopsis mesophyll protoplasts: a versatile
782 cell system for transient gene expression analysis. *Nat Protoc*, **2**, 1565-1572.
783

784

FIGURE LEGENDS

Figure 1. SnRK1 is SUMOylated

(a) Multiple SnRK1 subunits are SUMOylated in a heterologous *E. coli* system. SnRK1 subunits harboring 6*His and T7 tags were co-expressed in *E. coli* with the indicated SUMO isoform together with the SUMO-activating (AtSAE1a/AtSAE2) and SUMO-conjugating (AtSCE1) enzymes. SnRK1 subunits were purified *via* their His tag by IMAC and immunoblotted against their T7 tag ("WB: T7"). GG and AA refer to conjugatable and non-conjugatable SUMO variants, respectively. Equal protein loading is shown by Coomassie Blue (*CB*) staining of membranes. (b and c) The SnRK1 complex is SUMOylated *in planta*. Leaf crude extracts of plants expressing GFP (Ctrl), SnRK1α1ΔKA1-GFP (Δ) and full length SnRK1α1-GFP (FL) were used for GFP immunoprecipitation (IP) and immunoprecipitates were analyzed by Western-Blot (WB) using antibodies against GFP, SnRK1α1 and SUMO1 (b) or against SnRK1α1, SnRK1β1, SnRK1βγ and SUMO1 (c). The same antibodies were used for assessing the levels of these proteins in the corresponding inputs. Note that in Ctrl plants GFP is driven by the strong *35S* promoter whereas SnRK1α1ΔKA1-GFP and SnRK1α1-GFP are driven by the *SnRK1α1* promoter, hence explaining why GFP can only be detected in the input of *35S::GFP* plants. Black and grey arrowheads: non-SUMOylated and SUMOylated proteins, respectively. Grey brackets: high molecular weight forms of the indicated proteins.

Figure 2. SIZ1-mediated SUMOylation of SnRK1 represses SnRK1 signaling

(a) Normal induction of SnRK1 signaling by SnRK1α1 multiple-lysine mutants. Expression of SnRK1α1 in Arabidopsis mesophyll protoplasts triggers SnRK1 signaling, as measured by induction of the *pDIN6::LUC* reporter. Mutation of lysine residues found to be SUMOylated

in the *E. coli* system does not alter the ability of SnRK1α1 to induce the *pDIN6::LUC* reporter. SnRK1^{3K}, K34R/K63R/K390R; SnRK1^{8K}, K20R/K34R/K44R/K56R/K63R/K69R/K390R/K421R. An inactive T-loop phospho-mutant (SnRK1α1^{T175A}) is used as negative control. (b) SIZ1 is required for SnRK1 SUMOylation. SnRK1α1-GFP was immunoprecipitated (IP) from leaf crude extracts of SnRK1α1-GFP ("WT") and SnRK1α1-GFP$_{siz1-2}$ ("*siz1-2*") and analyzed by Western-Blot (WB) using antibodies against SnRK1α1 and SUMO1 (as in Figure 1b). The amounts of loaded immunoprecipitates were adjusted to contain approximately similar amounts of SnRK1α1-GFP in WT and *siz1-2*. The quantification of hMW SnRK1α1 forms in both genotypes is presented on the right and corresponds to the ratio of hMW forms (indicated with a bracket in the longer exposure, "long") per unmodified SnRK1α1 (shorter exposure, "short"). The values are normalized to the ratio in control plants ("WT"). (c) Overinduction of SnRK1 signaling in the *siz1-2* mutant. Relative gene expression (qPCR) of SnRK1 marker genes (*AXP, DIN6, TPS8*) in Col-0 or *siz1-2* mutant plants treated under control (Light) or energy stress (Dark) conditions. (d) Overinduction of SnRK1 signaling in *siz1-2* is rescued by the catalytic activity of SIZ1. Expression of SnRK1α1 triggers a three-fold higher induction of the *pDIN6::LUC* reporter in *siz1-2* than in Col-0 protoplasts. Normal *pDIN6::LUC* expression is recovered by co-expression of SIZ1, but not of a catalytically inactive SIZ1^{C379A} variant. (e) Induction of SnRK1 signaling downstream of SnRK1 is normal in *siz1-2*. Expression of the GBF5 transcription factor triggers similar induction of the *pDIN6::LUC* reporter in Col-0 and *siz1-2* protoplasts. Expression of all components was confirmed by Western Blot (WB) with anti-HA antibodies. Equal sample loading was confirmed by Coomassie Blue (CB) staining of RubisCO Large subunit on membranes. Data are presented as mean ± SEM. Statistical significance was determined by ratio pair *t*-test prior to normalization (b), paired *t*-test (c), and two-way ANOVA (d). n≥3; ns, p>0.05; * p<0.05; **p<0.01; ****p<0.0001.

Figure 3. SnRK1 stability is increased in *siz1-2*

(a) SnRK1 specific activity is not altered in the *siz1-2* mutant. SnRK1α1 was immunoprecipitated from Col-0 and *siz1-2* leaf extracts and incubated in the presence of γ-^{32}P-ATP and a recombinant ABF2 polypeptide as substrate. SnRK1α1 levels and ABF2 phosphorylation were quantified by Western-blot (WB) and by autoradiography (P-ABF2), respectively. (b and c) SnRK1 accumulates to higher levels in the *siz1-2* mutant. Total leaf protein extracts of Col-0 and *siz1-2* plants were analyzed by Western-blot (WB) using antibodies against SnRK1α1 (”α1”) and the phosphorylated T-loop of SnRK1α1 and SnRK1α2 (”P-α1/P-α2”) (b, 10 or 17 µg) or against the SnRK1β1 subunit (c, 20 µg). The signals were quantified and normalized to loading. The average quantification in *siz1-2* normalized to Col-0 is presented. (d) Reduced SnRK1α1 degradation in *siz1-2* is restored in a SUMO-mimetic SnRK1α1 variant. SnRK1α1 fused to mature SUMO1 (-mS1, empty marks) or not (WT, filled marks) was expressed in Col-0 (squares) or *siz1-2* (circles) protoplasts. Protoplasts were thereafter treated with cycloheximide (CHX), samples were harvested at the indicated times points, and analyzed by Western-blot using anti-SnRK1α1 antibody (WB: α1). The signal was quantified and normalized to the t=0 for each kinetics. (e) Restoring SnRK1 SUMOylation in the *siz1-2* mutant by expression of the SUMO-mimetic SnRK1α1 variant (α1-mS1) results in normal activation of the *pDIN6::LUC* reporter. Expression of all SnRK1α1 variants was confirmed by Western Blot (WB) with anti-SnRK1α1 antibodies. Equal sample loading was confirmed by Coomassie Blue (CB) staining of RubisCO Large subunit on membranes. Data are presented as mean ± SEM. Statistical significance was determined by ratio paired *t*-test prior to normalization (b and c) or by ANOVA (d, e). n≥3; ns, p>0.05; *p<0.05; **p<0.01; ****p<0.0001.

Figure 4. SUMOylated SnRK1 is ubiquitinated and degraded by the proteasome

(a) SnRK1α1 is degraded through the proteasome. SnRK1α1 was expressed in Col-0 protoplasts and its levels were assessed by Western-blot (WB) following a 3h treatment with cycloheximide (CHX) in the presence or absence of the proteasome inhibitor MG132. Equal sample loading was confirmed by Coomassie Blue (CB) staining of RubisCO Large subunit on membranes. Quantified levels were normalized to t=0. Data are presented as mean ± SEM. Statistical significance was determined by ratio pair *t*-test prior to data normalization. n≥3; **p<0.01; *p<0.05. (b) The SnRK1 complex is ubiquitinated *in planta*. Leaf crude extracts of plants expressing GFP (Ctrl), SnRK1α1ΔKA1-GFP (Δ) and full length SnRK1α1-GFP (FL) were used for GFP immunoprecipitation (IP) and immunoprecipitates were analyzed by Western-Blot (WB) using antibodies against SnRK1α1 and Ubiquitin11. The same antibodies were used for assessing the levels of these proteins in the corresponding inputs. (c) SnRK1 ubiquitination is largely dependent on SIZ1. SnRK1α1-GFP was immunoprecipitated (IP) from leaf crude extracts of SnRK1α1-GFP ("WT") and SnRK1α1-GFP$_{siz1\text{-}2}$ ("*siz1-2*") and analyzed by Western-Blot (WB) using antibodies against SnRK1α1 and Ubiquitin11. The amounts of loaded immunoprecipitates were adjusted to contain approximately similar amounts of SnRK1α1-GFP in WT and *siz1-2*.

Figure 5. Degradation of SnRK1 requires its activity

(a) Inactive SnRK1α1 variants accumulate to higher levels than the WT protein. Accumulation of WT SnRK1α1 and two inactive SnRK1α^{1T175A} and SnRK1α1^{K48M} mutants transiently expressed in Col-0 protoplasts was analyzed by Western-blot using anti-SnRK1α1 antibodies (WB: α1). (b) Only active SnRK1α1 undergoes degradation. WT (squares) or inactive (circles) SnRK1α1 variants were expressed in Col-0 protoplasts. Protoplasts were thereafter treated with cycloheximide (CHX), samples were harvested at the indicated time

885 points, and analysed by Western-blot using anti-SnRK1α1 antibodies (WB: α1). The signal
886 was quantified and normalized to the t=0 for each kinetics. (c) Inactive SnRK1α1 variants
887 undergo degradation when expressed as SUMO-mimetics. Levels of SnRK1α1-mature
888 SUMO1 (mS1) fusions were followed as in (b). The SnRK1α1 variants used as mS1 fusions
889 are indicated (WT, squares; T175A, red circles, K48M, blue circles). GFP fused to mS1 is
890 provided as a negative control (green triangles). Data are presented as mean ± SEM.
891 Statistical significance was determined by two-way ANOVA with Tukey's multiple
892 comparison. n≥3; *p<0.05, **p<0.01; ***p<0.001.
893
894 **Figure 6. Model of SnRK1 regulation by SUMOylation**
895 Active SnRK1 regulates processes that promote energy homeostasis. As a consequence of its
896 activity SnRK1 is SUMOylated on several subunits in a SIZ1-dependent manner,
897 ubiquitinated, and degraded through the proteasome. The tight coupling between SnRK1
898 activity and degradation may contribute to establishing a balance between stress/defense
899 responses and biosynthetic growth-related processes.
900
901
902

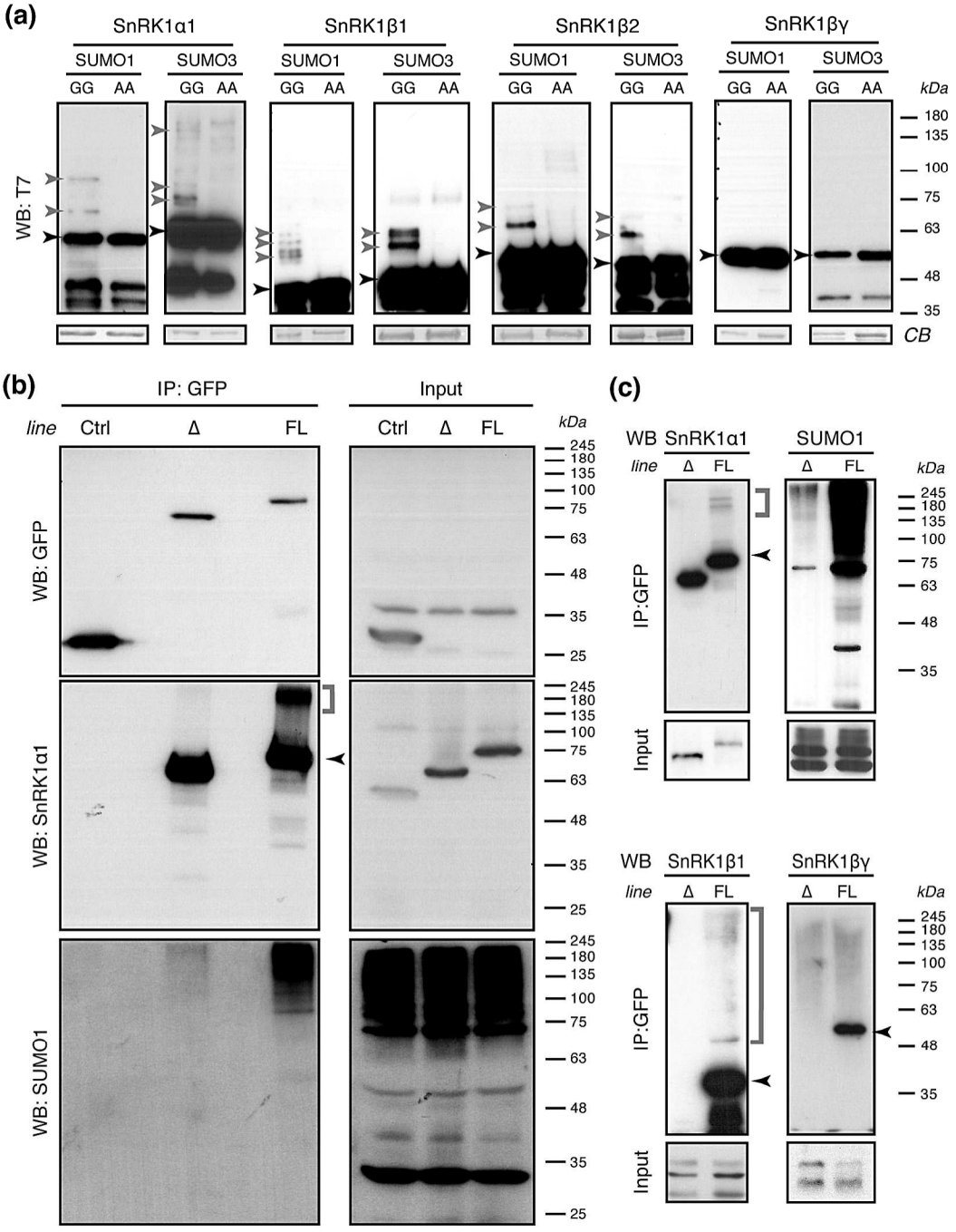

Figure 1. SnRK1 is SUMOylated.

(a) Multiple SnRK1 subunits are SUMOylated in a heterologous *E. coli* system. SnRK1 subunits harboring 6*His and T7 tags were co-expressed in *E. coli* with the indicated SUMO isoform together with the SUMO-activating (AtSAE1a/AtSAE2) and SUMO-conjugating (AtSCE1) enzymes. SnRK1 subunits were purified *via* their His tag by IMAC and immunoblotted against their T7 tag ("WB: T7"). GG and AA refer to conjugatable and non-conjugatable SUMO variants, respectively. Equal protein loading is shown by Coomassie Blue (CB) staining of membranes. (b and c) The SnRK1 complex is SUMOylated *in planta*. Leaf crude extracts of plants expressing GFP (Ctrl), SnRK1α1ΔKA1-GFP (Δ) and full length SnRK1α1-GFP (FL) were used for GFP immunoprecipitation (IP) and immunoprecipitates were analyzed by Western-Blot (WB) using antibodies against GFP, SnRK1α1 and SUMO1 (b) or against SnRK1α1, SnRK1β1, SnRK1βγ and SUMO1 (c). The same antibodies were used for assessing the levels of these proteins in the corresponding inputs. Note that in Ctrl plants GFP is driven by the strong 35S promoter whereas SnRK1α1ΔKA1-GFP and SnRK1α1-GFP are driven by the SnRK1α1 promoter, hence explaining why GFP can only be detected in the input of 35S::GFP plants. Black and grey arrowheads: non-SUMOylated and SUMOylated proteins, respectively. Grey brackets: high molecular weight forms of the indicated proteins.

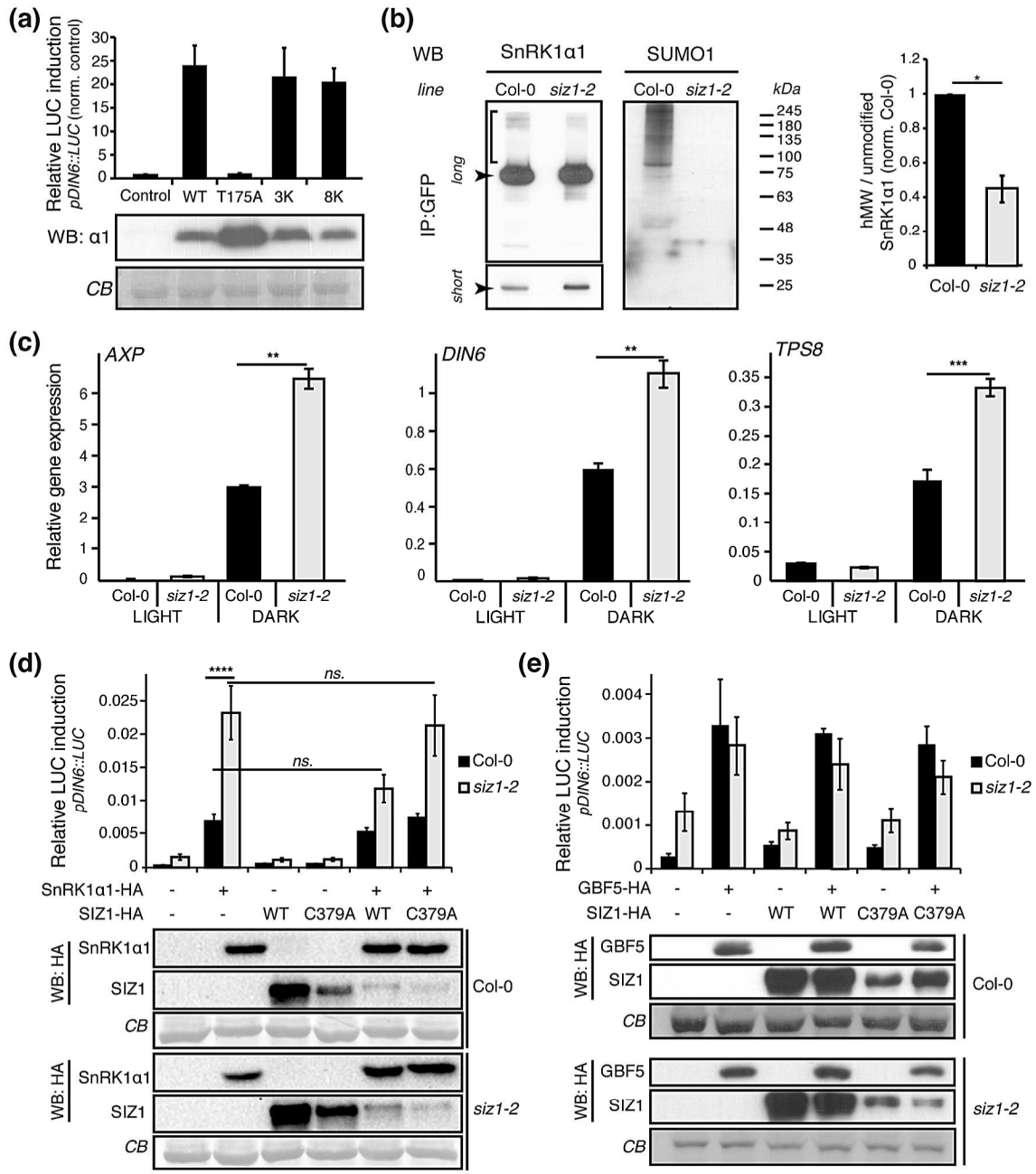

Figure 2. SIZ1-mediated SUMOylation of SnRK1 represses SnRK1 signaling.
(a) Normal induction of SnRK1 signaling by SnRK1α1 multiple-lysine mutants. Expression of SnRK1α1 in Arabidopsis mesophyll protoplasts triggers SnRK1 signaling, as measured by induction of the *pDIN6::LUC* reporter. Mutation of lysine residues found to be SUMOylated in the *E. coli* system does not alter the ability of SnRK1α1 to induce the *pDIN6::LUC* reporter. SnRK1^{3K}, K34R/K63R/K390R; SnRK1^{8K}, K20R/K34R/K44R/K56R/K63R/K69R/K390R/K421R. An inactive T-loop phospho-mutant (SnRK1α1^{T175A}) is used as negative control. (b) SIZ1 is required for SnRK1 SUMOylation. SnRK1α1-GFP was immunoprecipitated (IP) from leaf crude extracts of SnRK1α1-GFP ("WT") and SnRK1α1-GFP$_{siz1-2}$ ("*siz1-2*") and analyzed by Western-Blot (WB) using antibodies against SnRK1α1 and SUMO1 (as in Figure 1b). The amounts of loaded immunoprecipitates were adjusted to contain approximately similar amounts of SnRK1α1-GFP in WT and *siz1-2*. The quantification of hMW SnRK1α1 forms in both genotypes is presented on the right and corresponds to the ratio of hMW forms (indicated with a bracket in the longer exposure, "long") per unmodified SnRK1α1 (shorter exposure, "short"). The values are normalized to the ratio in control plants ("WT"). (c) Overinduction of SnRK1 signaling in the *siz1-2* mutant. Relative gene expression (qPCR) of SnRK1 marker genes (*AXP*, *DIN6*, *TPS8*) in Col-0 or *siz1-2* mutant plants treated under control (Light) or energy stress (Dark) conditions. (d) Overinduction of SnRK1 signaling in *siz1-2* is rescued by the catalytic activity of SIZ1. Expression of SnRK1α1 triggers a three-fold higher induction of the *pDIN6::LUC* reporter in *siz1-2* than in Col-0 protoplasts. Normal *pDIN6::LUC* expression is recovered by co-expression of SIZ1, but not of a catalytically inactive SIZ1^{C379A} variant. (e) Induction of SnRK1 signaling downstream of SnRK1 is normal in *siz1-2*. Expression of the GBF5 transcription factor triggers similar induction of the *pDIN6::LUC* reporter in Col-0 and *siz1-2* protoplasts. Expression of all components was confirmed by Western Blot (WB) with anti-HA antibodies. Equal sample loading was confirmed by Coomassie Blue (CB) staining of RubisCO Large subunit on membranes. Data are presented as mean ± SEM. Statistical significance was determined by ratio pair *t*-test prior to normalization (b), paired *t*-test (c), and two-way ANOVA (d). n≥3; ns, p>0.05; * p<0.05; **p<0.01; ****p<0.0001.

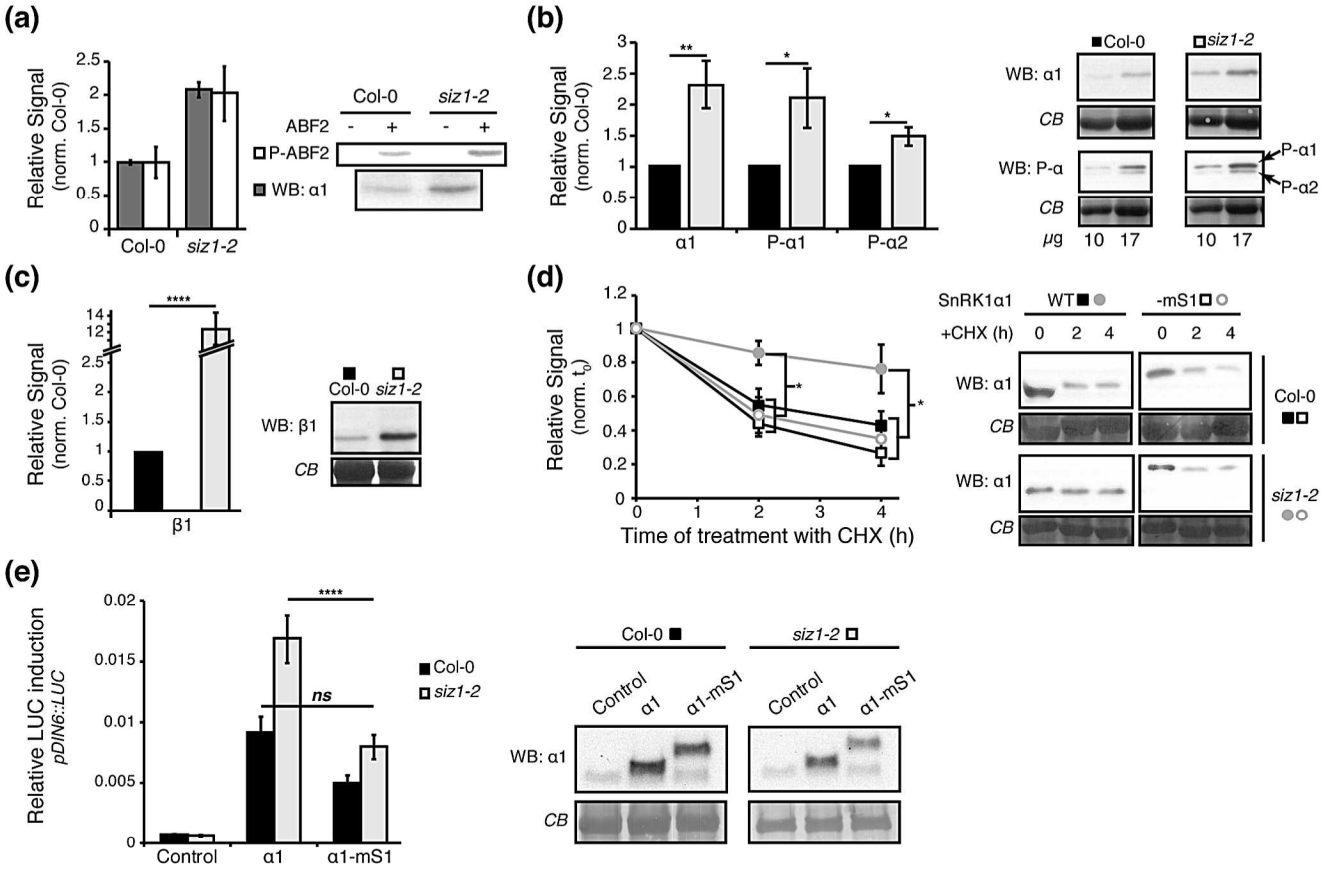

Figure 3. SnRK1 stability is increased in *siz1-2*

(a) SnRK1 specific activity is not altered in the *siz1-2* mutant. SnRK1α1 was immunoprecipitated from Col-0 and *siz1-2* leaf extracts and incubated in the presence of γ-^{32}P-ATP and a recombinant ABF2 polypeptide as substrate. SnRK1α1 levels and ABF2 phosphorylation were quantified by Western-blot (WB) and by autoradiography (P-ABF2), respectively. (b and c) SnRK1 accumulates to higher levels in the *siz1-2* mutant. Total leaf protein extracts of Col-0 and *siz1-2* plants were analyzed by Western-blot (WB) using antibodies against SnRK1α1 ("α1") and the phosphorylated T-loop of SnRK1α1 and SnRK1α2 ("P-α 1/P-α2") (b, 10 or 17 *μ*g) or against the SnRK1β1 subunit (c, 20 *μ*g). The signals were quantified and normalized to loading. The average quantification in *siz1-2* normalized to Col-0 is presented. (d) Reduced SnRK1α1 degradation in *siz1-2* is restored in a SUMO-mimetic SnRK1α1 variant. SnRK1α1 fused to mature SUMO1 (-mS1, empty marks) or not (WT, filled marks) was expressed in Col-0 (squares) or *siz1-2* (circles) protoplasts. Protoplasts were thereafter treated with cycloheximide (CHX), samples were harvested at the indicated times points, and analyzed by Western-blot using anti-SnRK1α1 antibody (WB: α1). The signal was quantified and normalized to the t=0 for each kinetics. (e) Restoring SnRK1 SUMOylation in the *siz1-2* mutant by expression of the SUMO-mimetic SnRK1α1 variant (α1-mS1) results in normal activation of the *pDIN6::LUC* reporter. Expression of all SnRK1α1 variants was confirmed by Western Blot (WB) with anti-SnRK1α1 antibodies. Equal sample loading was confirmed by Coomassie Blue (CB) staining of RubisCO Large subunit on membranes. Data are presented as mean ± SEM. Statistical significance was determined by ratio paired *t*-test prior to normalization (b and c) or by ANOVA (d, e). n≥3; ns, p>0.05; *p<0.05; **p<0.01; ****p<0.0001.

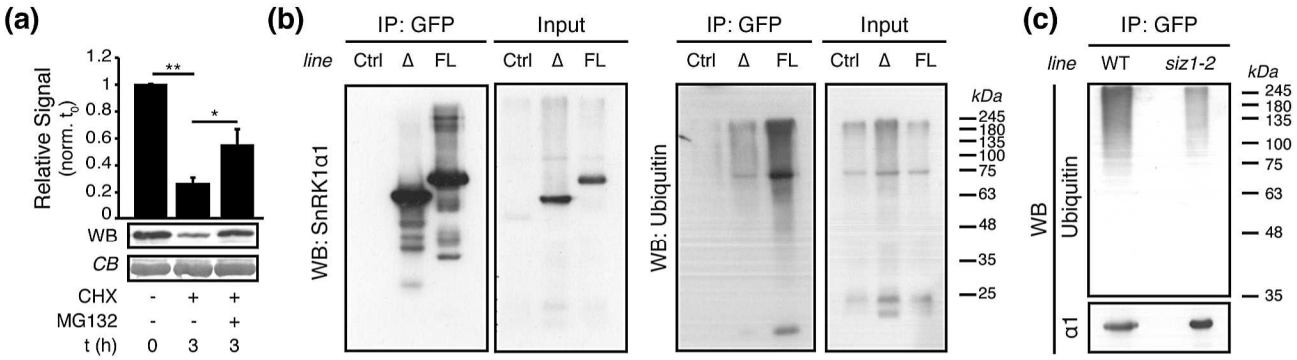

Figure 4. SUMOylated SnRK1 is ubiquitinated and degraded by the proteasome

(a) SnRK1α1 is degraded through the proteasome. SnRK1α1 was expressed in Col-0 protoplasts and its levels were assessed by Western-blot (WB) following a 3h treatment with cycloheximide (CHX) in the presence or absence of the proteasome inhibitor MG132. Equal sample loading was confirmed by Coomassie Blue (CB) staining of RubisCO Large subunit on membranes. Quantified levels were normalized to t=0. Data are presented as mean ± SEM. Statistical significance was determined by ratio pair *t*-test prior to data normalization. n≥3; **p<0.01; *p<0.05. (b) The SnRK1 complex is ubiquitinated *in planta*. Leaf crude extracts of plants expressing GFP (Ctrl), SnRK1α1ΔKA1-GFP (Δ) and full length SnRK1α1-GFP (FL) were used for GFP immunoprecipitation (IP) and immunoprecipitates were analyzed by Western-Blot (WB) using antibodies against SnRK1α1 and Ubiquitin11. The same antibodies were used for assessing the levels of these proteins in the corresponding inputs. (c) SnRK1 ubiquitination is largely dependent on SIZ1. SnRK1α1-GFP was immunoprecipitated (IP) from leaf crude extracts of SnRK1α1-GFP ("WT") and SnRK1α1-GFP$_{siz1-2}$ ("*siz1-2*") and analyzed by Western-Blot (WB) using antibodies against SnRK1α1 and Ubiquitin11. The amounts of loaded immunoprecipitates were adjusted to contain approximately similar amounts of SnRK1α1-GFP in WT and *siz1-2*.

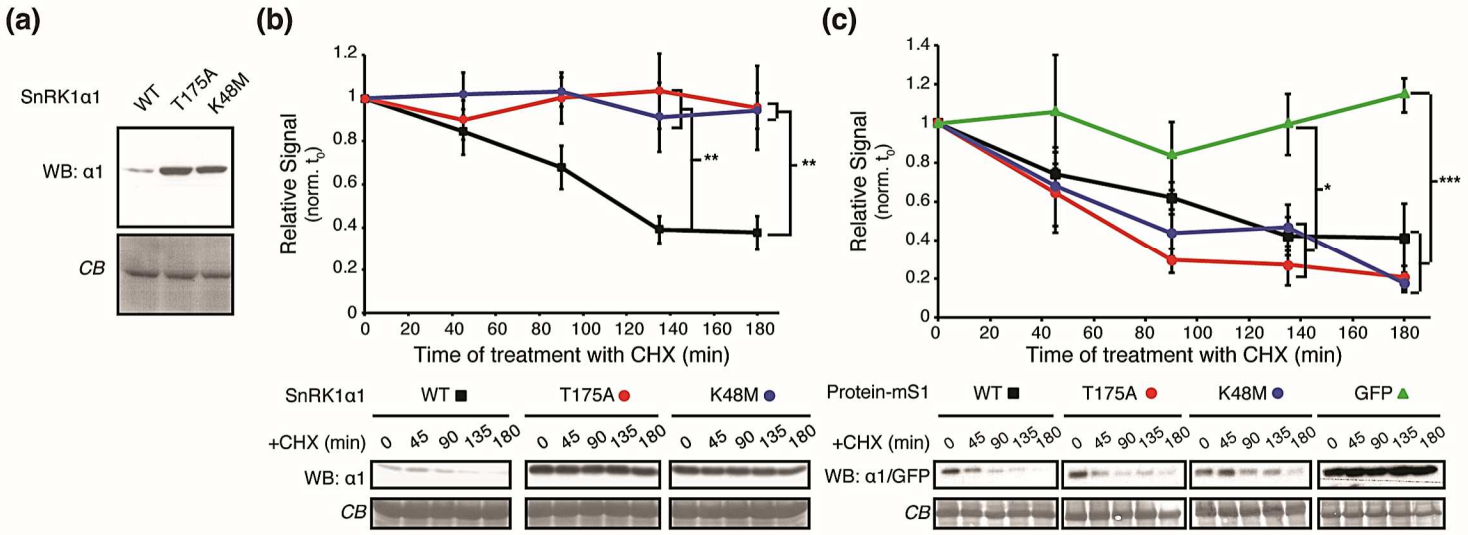

Figure 5. Degradation of SnRK1 requires its activity

(a) Inactive SnRK1α1 variants accumulate to higher levels than the WT protein. Accumulation of WT SnRK1α1 and two inactive SnRK1α1^{T175A} and SnRK1α1^{K48M} mutants transiently expressed in Col-0 protoplasts was analyzed by Western-blot using anti-SnRK1α1 antibodies (WB: α1). (b) Only active SnRK1α1 undergoes degradation. WT (squares) or inactive (circles) SnRK1α1 variants were expressed in Col-0 protoplasts. Protoplasts were thereafter treated with cycloheximide (CHX), samples were harvested at the indicated time points, and analysed by Western-blot using anti-SnRK1α1 antibodies (WB: α1). The signal was quantified and normalized to the t=0 for each kinetics. (c) Inactive SnRK1α1 variants undergo degradation when expressed as SUMO-mimetics. Levels of SnRK1α1-mature SUMO1 (mS1) fusions were followed as in (b). The SnRK1α1 variants used as mS1 fusions are indicated (WT, squares; T175A, red circles, K48M, blue circles). GFP fused to mS1 is provided as a negative control (green triangles). Data are presented as mean ± SEM. Statistical significance was determined by two-way ANOVA with Tukey's multiple comparison. n≥3; *p<0.05, **p<0.01; ***p<0.001.

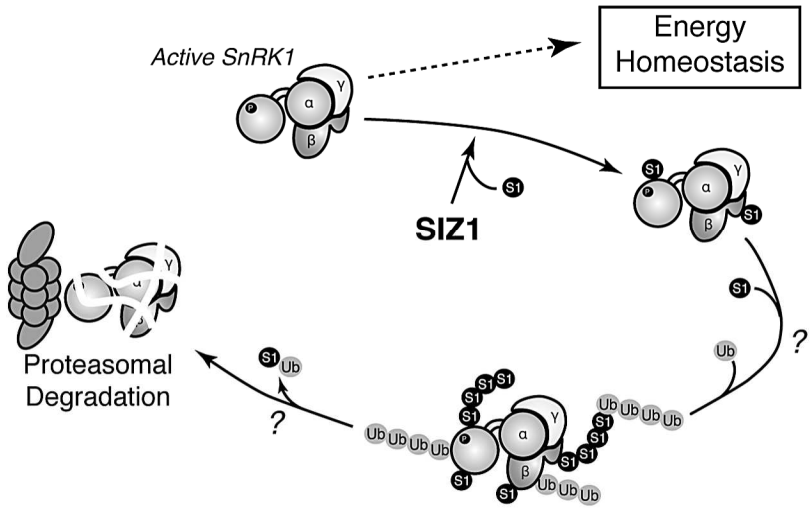

Figure 6. Model of SnRK1 regulation by SUMOylation.
Active SnRK1 regulates processes that promote energy homeostasis. As a consequence of its activity SnRK1 is SUMOylated on several subunits in a SIZ1-dependent manner, ubiquitinated, and degraded through the proteasome. The tight coupling between SnRK1 activity and degradation may contribute to establishing a balance between stress/defense responses and biosynthetic growth-related processes.

METHODS S1

Cloning and site-directed mutagenesis

All cloning steps and primers are detailed in Table S1.

To generate point mutations, PCR was performed using primers carrying the intended mutation and annealing to the same sequence on opposite strands of the original plasmid template. A 25µl reaction mix [primers (25ng each), template plasmid (50ng), 250µM of dNTPs, Pfu polymerase (1.25U, Promega M7745) and 1X Pfu buffer] was split in two tubes (12.5µl each); one was incubated in a thermocycler [95°C – 3min; (95°C-30s, 55°C-40s, 68°C-2min/kb) x 14] while the other was kept at 4°C. Ten units of DpnI (NEB) were thereafter added to both and incubated at 37°C for 12h prior to bacteria transformation (4µL typically used). Positive clones were always confirmed by sequencing.

Y2H Assays

Y2H assays were performed as described (Saez *et al.* 2008). The full-length coding sequence of SnRK1α1 and the various deletions were cloned into pGADT7 in fusion with the GAL4 activation domain. pGADT7 constructs were faced with pGBKT7 harboring full-length SCE1 fused to the DNA binding domain of GAL4. The empty vectors were used as negative controls.

E. coli heterologous SUMOylation assay

Analyses of SnRK1 SUMOylation in *E. coli* were performed as described with slight modifications (Okada *et al.* 2009). pET28a was used to express potential SUMO targets (SnRK1α1 and its truncated and mutant variants, SnRK1β1, SnRK1β2, SnRK1γ and SnRK1βγ). BL21(DE3) cells were transformed with pACYCDuet-AtSAE1a-AtSAE2 and selected on 34µg/ml chloramphenicol (Cm) LB Agar plates. 100µl of pACYCDuet-AtSAE1a-AtSAE2 transformed BL21(DE3) competent cells were co-transformed with 30-50ng of pCDFDuet-AtSUMO1/3(AA or GG)-AtSCE1a and pET28a-SnRK1α1 (and its truncation and mutation variants)/SnRK1β1/SnRK1β2/SnRK1γ/SnRK1βγ and then selected on 17µg/mL Cm, 15µg/mL Kanamycin (Kan) and 25µg/mL Spectinomycin (Spec) LB Agar plates. Transformed cells were incubated in 34µg/mL Cm, 30µg/mL Kan and 50µg/mL Spec LB liquid media at 25°C, 200rpm, until Abs^{600nm} reached 0.5-0.8. The

expression of recombinant proteins was induced with 0.15mM IPTG (PROMV3955, Promega) at 25 °C for 12h.

For analyzing total soluble proteins, cells were harvested from 3mL cultures and lysed with 100µL of BugBuster Protein Extraction Reagent (Novagen) supplemented with 2µL of ProteoBlock (#R1321, Fermentas), 2µL of Lysozyme (L1667, Sigma) and 2µL of DNAse (PROMM6101, Promega). Samples were incubated 20min at RT and cleared by centrifugation (20,000g, 4°C, 25 min). About 100µg of soluble protein (estimated by Abs^{280nm}) were subjected to SDS-PAGE and immunoblotting with an anti-T7 antibody.

For analyses from purified proteins, bacteria were pelleted at 4000g for 30min at 4°C, resuspended in Lysis buffer [50mM Hepes-NaOH pH7.25, 0.1M NaCl, antiprotease cOmplete without EDTA (1 tablet/50mL)] and sonicated. After centrifugation (20,000g for 30min at 4°C) the soluble fraction was subjected to IMAC purification (Ni-NTA agarose, Qiagen, 30210). Beads were pre-equilibrated in Lysis buffer and incubated with the soluble protein extract under gentle shaking for 1h at RT. Beads were thereafter washed under gravity flow with Lysis buffer (5 BV, bed volume) and then with 50mM Hepes-NaOH pH7.25 until Abs^{230nm} reached 0 or stabilized at less than 0.1. A final wash was applied with 50mM Hepes-NaOH pH7.25, 20mM imidazole. Three consecutive elutions with 50mM Hepes-NaOH pH7.25 supplemented with 100, 200 or 500mM of imidazole were performed during at least 20min at RT under gentle shaking. Eluates were loaded on 30kDa Amicon columns (Millipore) for buffer exchange (to reach a 20mM imidazole concentration) and protein concentration, and were thereafter analyzed (20µg) by SDS-PAGE and immunoblotting with anti-T7.

Mass spectrometry analyses

For Mass spectrometry analyses of SUMOylated SnRK1α1-KD and SnRK1α1-RD (using SUMO3-GG or a $SUMO3^{S91R}$-GG variant), 15-30µg of concentrated eluates (see previous section) were resolved on SDS-PAGE (8%), stained with Coomassie Brilliant Blue R250 (VWR: 443283M, 0.2% w/V in 14% Acetic Acid, 14% ethanol), and destained (10% Acetic Acid, 25% ethanol) until the bands were clearly visible. Bands were excised, alkylated with iodoacetamide (carbamidomethylation of cysteines), and digested with trypsin. Eluted peptides were separated by liquid chromatography and detected with an Orbitrap Velos Pro Hybrid Ion Trap Mass Spectrometer (Thermo Scientific). An initial hit

search was done in the NCBI non-redundant database with "Arabidopsis thaliana" as a query organism. Approximately 3400 queries were made for each sample, with peptide mass tolerance ± 3 ppm and fragment mass tolerance ± 0.8 Da. For a more refined validation, a micro-database was created containing *in silico* predicted masses of the branched peptides resulting from SUMOylation was compared manually to the data set.

Generation of *SnRK1α1-GFP*, *SnRK1α1ΔKA1-GFP and SnRK1α1-GFP*$_{siz1-2}$ and *35S::GFP* lines

A homozygous insertion line for the *SnRK1α1* gene (At3g01090), was identified in the GABI-KAT collection (GABI_579E09; Figure S3) and was designated as *snrk1α1-3* [previously described *snrk1α1-1* and *snrk1α1-2* mutants are not null (Tsai and Gazzarrini 2012)]. Genotyping was performed using primers *snrk1α1*-GABIa and *snrk1α1*-GABIb in combination with a left border T-DNA primer (GABI-08409-LB). To determine the T-DNA exact insertion site, a genomic DNA fragment was amplified by PCR with a forward primer binding to the *SnRK1α1* locus (SnRK1α1-seqF Fw) and a reverse primer binding to the T-DNA right border (GABI1-RB-seq Rv). Sequencing reactions were subsequently performed on the gel-purified PCR product using the same primers. The T-DNA insertion was mapped to position 2583-2593, immediately before the last exon. The last 11 bases of the intron at the insertion site are missing. The potential presence of a second insertion in the *IMS2* gene (AT5G23020), as annotated in the GABI-Kat site, was ruled out by genotyping with primers IMS2-Fw and IMS2-Rv in combination with the GABI-08409-LB primer. The absence of SnRK1α1 protein in *snrk1α1-3* plants was confirmed by immunoblotting with antibodies recognizing epitopes well before the T-DNA insertion, a SnRK1α1-specific antibody and an AMPKα-pT172 antibody recognizing the phosphorylated T-loop of SnRK1α1 and SnRK1α2 [T175 and T176, respectively; (Baena-Gonzalez *et al.* 2007)].

The *pSnRK1α1::SnRK1α1-GFP::tSnRK1α1* and *pSnRK1α1::SnRK1α1ΔKA1-GFP::tSnRK1α1* constructs are in the pBm43GW,0 MultiSite Gateway Binary vector (Karimi *et al.* 2005) and the corresponding areas of the gene are indicated in Figure S3A. Both constructs were generated using a pDONR-P4P1R harboring the *SnRK1α1* upstream regulatory region (*pSnRK1α1*, 2000 bp upstream of the *SnRK1α1* start codon in the At3g01090.2 gene model; amplified using primers PROM-5'UTR_gSnRK1α1 attB4 Fw and PROM-5'UTR_gSnRK1α1 attB1r Rv) and a pDONR-P2RP3 harboring the

SnRK1α1 downstream regulatory region (*tSnRK1α1*, 1000 bp downstream of the *SnRK1α1* stop codon in the At3g01090.2 gene model; amplified using primers TERM-3'UTR_gSnRK1α1 attB2r Fw and TERM-3'UTR_gSnRK1α1 attB3 Rv). In *pSnRK1α1::SnRK1α1-GFP::tSnRK1α1* the middle pDONR221-P1P2 contained the full genomic sequence of *SnRK1α1* fused to GFP (primers gSnRK1α1-GFP attB1 Fw and gSnRK1α1-GFP attB2 Rv), whereas in *pSnRK1α1::SnRK1α1ΔKA1-GFP::tSnRK1α1,* it contained the coding sequence of *SnRK1α1* truncated at the KA1 domain and fused to GFP (primers gSnRK1α1-GFP attB1 Fw and gSnRK1α1-GFP attB2 Rv). The *pSnRK1α1::SnRK1α1-GFP::tSnRK1α1* and *pSnRK1α1::SnRK1α1ΔKA1-GFP:tSnRK1α1* constructs were introduced into *Agrobacterium tumefaciens* (GV3101) and *snrk1α1-3 or siz1-2* plants were transformed by the floral dip method (Clough and Bent 1998) to generate *pSnRK1α1::SnRK1α1-GFP::tSnRK1α1/snrk1α1-3* (referred as *SnRK1α1-GFP*), *pSnRK1α1::SnRK1α1ΔKA1-GFP::tSnRK1α1/snrk1α1-3* (referred as *SnRK1α1ΔKA1-GFP*), and *pSnRK1α1::SnRK1α1-GFP::tSnRK1α1/siz1-2* (referred as $SnRK1\alpha1\text{-}GFP_{siz1\text{-}2}$). BASTA-resistant transformants were selected based on their segregation ratio (T2) and homozygosity (T3). Homozygous T3 or T4 generation transgenic lines were used.

For the generation of plants with constitutive GFP expression (*35S::GFP*), Col-0 plants were transformed with a pBA vector (Duque and Chua 2003) for expression of GFP under the Cauliflower Mosaic Virus *35S* promoter.

Recombinant Protein Production and Purification

Recombinant His-ΔC ABF2 (residues 1–173) was produced and purified as previously described (Rodrigues *et al.* 2013). Successful protein production and purification was verified by immunoblotting with an anti-T7 antibody.

Endogenous protein quantification

Leaves of 5-week-old Col-0 and *siz1-2* plants were grounded in liquid nitrogen and resuspended in Buffer C. After two successive centrifugations (20,000g, 4°C, 10min), the supernatant was recovered and filtered (0.45µm), and total protein was quantified using the Bradford protein assay (Bio-Rad; #5000006). Equal protein amounts from the three extracts were solubilized with Laemmli buffer (Laemmli 1970), resolved by SDS-PAGE (8%), transferred to a PVDF membrane at 15V for 1h (semi-dry transfer, Bio-Rad) and immunodetected using antibodies against specific SnRK1 subunits.

Quantification of immunoblot results

Membranes were analyzed by immunoblotting and then stained with Coomassie Brilliant Blue R250. Band intensity was quantified using Image J (http://imagej.nih.gov/ij/) and GelQuantNet (http://biochemlabsolutions.com/GelQuantNET.html) softwares. The immunoblot intensities were normalized to the Coomassie staining intensity (referred as "loading"). In Figures 3, 4 and 5 quantifications were normalized to the t=0 of each kinetics or to Col-0 for Figure 3B and C.

Statistical Analyses

All statistical analyses were performed with the GraphPad Prism 6 software (GraphPad softwares). For analyses of qPCR data, the statistical significance of the indicated changes was assessed employing $\log_2$-transformed relative expression values (Rieu and Powers 2009).

Chemicals

Cycloheximide (Sigma, C7698; ethanol stock), MG132 (Sigma, C2211; DMSO stock) and Salicylic Acid (Aldrich: 105910; ethanol stock) solutions were always freshly prepared and used at a final concentration of 100µM, 50µM and 5µM, respectively.

SUPPLEMENTARY REFERENCES

Baena-Gonzalez, E., Rolland, F., Thevelein, J.M. and Sheen, J. (2007) A central integrator of transcription networks in plant stress and energy signalling. *Nature*, **448**, 938-942.

Clough, S.J. and Bent, A.F. (1998) Floral dip: a simplified method for Agrobacterium-mediated transformation of Arabidopsis thaliana. *Plant J*, **16**, 735-743.

Duque, P. and Chua, N.H. (2003) IMB1, a bromodomain protein induced during seed imbibition, regulates ABA- and phyA-mediated responses of germination in Arabidopsis. *Plant J*, **35**, 787-799.

Elrouby, N. and Coupland, G. (2010) Proteome-wide screens for small ubiquitin-like modifier (SUMO) substrates identify Arabidopsis proteins implicated in diverse biological processes. *Proc Natl Acad Sci U S A*, **107**, 17415-17420.

Karimi, M., De Meyer, B. and Hilson, P. (2005) Modular cloning in plant cells. *Trends Plant Sci*, **10**, 103-105.

Laemmli, U.K. (1970) Cleavage of structural proteins during the assembly of the head of bacteriophage T4. *Nature*, **227**, 680-685.

Okada, S., Nagabuchi, M., Takamura, Y., Nakagawa, T., Shinmyozu, K., Nakayama, J. and Tanaka, K. (2009) Reconstitution of Arabidopsis thaliana SUMO pathways in E. coli: functional evaluation of SUMO machinery proteins and mapping of SUMOylation sites by mass spectrometry. *Plant Cell Physiol*, **50**, 1049-1061.

Rieu, I. and Powers, S.J. (2009) Real-time quantitative RT-PCR: design, calculations, and statistics. *Plant Cell*, **21**, 1031-1033.

Rodrigues, A., Adamo, M., Crozet, P., Margalha, L., Confraria, A., Martinho, C., Elias, A., Rabissi, A., Lumbreras, V., Gonzalez-Guzman, M., Antoni, R., Rodriguez, P.L. and Baena-Gonzalez, E. (2013) ABI1 and PP2CA Phosphatases Are Negative Regulators of Snf1-Related Protein Kinase1 Signaling in Arabidopsis. *Plant Cell*, **25**, 3871-3884.

Saez, A., Rodrigues, A., Santiago, J., Rubio, S. and Rodriguez, P.L. (2008) HAB1-SWI3B interaction reveals a link between abscisic acid signaling and putative SWI/SNF chromatin-remodeling complexes in Arabidopsis. *Plant Cell*, **20**, 2972-2988.

Simpson-Lavy, K.J. and Johnston, M. (2013) SUMOylation regulates the SNF1 protein kinase. *Proc Natl Acad Sci U S A*, **110**, 17432-17437.

Tsai, A.Y. and Gazzarrini, S. (2012) AKIN10 and FUSCA3 interact to control lateral organ development and phase transitions in Arabidopsis. *Plant J*, **69**, 809-821.

LEGENDS FOR SUPPLEMENTARY FIGURES

Figure S1. SnRK1α1 interacts with the SUMO E2 Conjugating Enzyme 1 (SCE1) in a Yeast two-Hybrid assay

The full-length coding sequence (FL), C-terminal Regulatory Domain (RD) encompassing the KA1 domain, or N-terminal Kinase Domain (KD) of SnRK1α1 (represented on the left), were cloned into pGADT7 in fusion with the GAL4 activation domain and co-transfected with pGBKT7 harboring either the GAL4 binding domain alone (empty) or in fusion with the full-length SCE1. The growth of transformed AH109 yeast cells was assessed in permissive [-Leucine (L), -Tryptophan (W)], selective [-L-W,-Histidine (H)], or more stringent [-L-W-H,-Adenine (A)] media. A representative experiment of a minimum of two independent assays is shown.

Figure S2. SnRK1γ is SUMOylated in *E. coli* and enriched in *siz1-2*, but is not part of the SnRK1α1 complex in Arabidopsis leaves

(a) SnRK1γ subunits containing 6*His and T7 tags were co-expressed in *E. coli* with SUMO3 together with the SUMO-activating (AtSAE1a/AtSAE2) and SUMO-conjugating

(AtSCE1) enzymes. After production, the protein from total lysate was immunoblotted against its T7 tag. GG and AA refer to conjugatable and non-conjugatable SUMO3 variants, respectively. Black and grey arrowheads mark non-SUMOylated and SUMOylated SnRK1γ, respectively. Equal protein loading is shown by Coomassie Blue (CB) staining of membranes. (b) SnRK1γ accumulates to higher levels in the *siz1-2* mutant. Total leaf protein extracts (10, 17, or 24 µg) of Col-0 and *siz1-2* plants were analyzed by Western-blot (WB) using antibodies against SnRK1γ. The signals were quantified and normalized to loading. The average quantification in *siz1-2* normalized to Col-0 is presented. Stars denote statistical significance, as determined by ratio paired *t*-test prior to normalization (n=3; error bars=SEM; *p<0.05). (c) Anti-GFP immunoprecipitation (IP) of SnRK1α1-GFP as in Figure 1b. The presence of SnRK1γ was assessed by immunodetection with SnRK1γ antibodies. Co-immunoprecipitation of SnRK1β1 was used as a positive control. The input corresponds to the soluble protein extracts that were used for IP. The black arrowheads indicate the SnRK1 subunits.

Figure S3. Generation of *SnRK1α1-GFP* transgenic lines

(a) Structure of the *SnRK1α1* gene (At3g01090.2 gene model). All indicated positions have the start codon (noted +1) as a reference. The promoter (2kb upstream of the start codon) and terminator (1 kb downstream of the stop codon) regions used, as well as the kinase and KA1 domains, are indicated. The location of the T-DNA insertion defining the *snrk1α1-3* mutant line (GABI-KAT: 579E09) is indicated as well as the position of the three genotyping primers (LP, Left Primer; RP, Right Primer; LB, Left Border; Supplementary Table 1). The sequence providing the exact location of the insertion (2583) in indicated inside the red box (”lost” denotes the 11 bases lost due to the insertion). White boxes correspond to exons. (b) Genotyping PCR using primers LP, RP, and LB, shown in (a). The expected sizes of the two products are indicated on the left (LP: LP-RP reaction, 386bp indicates WT allele; LB: LB-RP reaction, 190bp indicating a mutant allele). (c) Total proteins from adult Arabidopsis leaves of Col-0 or the *snrk1α1-3* mutant were analyzed by Western blot (WB) using antibodies against SnRK1α1, SnRK1α2 or P-AMPK (recognizing the phosphorylated T175/176 of SnRK1α1/α2, respectively). The black and grey arrowheads indicate phospho-SnRK1α1 and phospho-SnRK1α2, respectively. (d) Supporting data for Figure 1b. *SnRK1α1::GFP* transgenic lines were generated by transformation of the *snrk1α1-3* mutant with the pBm43GW,0

MultiSite Gateway Binary vector, containing the promoter (2 kb upstream of the start codon), the genomic coding region (exons-introns) and the terminator (1 kb downstream of the stop codon) of the *SnRK1α1* gene (At3g01090.2; indicated in (a). Several independent transgenic lines were tested for the presence of SnRK1α1-GFP by Western-blot (WB) using antibodies against SnRK1α1 and GFP. The selected lines (presenting a SnRK1α1 signal close to Col-0) are indicated with arrows. (e) *SnRK1α1ΔKA1::GFP* transgenic lines were generated using the CDS of *SnRK1α1* and analyzed as in (d). (f) Supporting data for Figure 2b. *SnRK1α1::GFP*$_{siz1-2}$ transgenic lines were generated by transformation of the *siz1-2* mutant with the pBm43GW,0 MultiSite Gateway Binary construct described in (d). Several transformants were tested for the presence of SnRK1α1-GFP by Western-blot (WB) using antibodies against SnRK1α1 and GFP. The selected lines are indicated with arrows. Equal protein loading in (c-f) is shown by Coomassie Blue (CB) staining of membranes.

Figure S4. SnRKα1 residues found SUMOylated in the *E. coli* assay

(a) Schematic representation of SnRK1α1 showing the regions referred thereafter. K48 (catalytic phospho-transfer) and T175 (activating T-loop phosphorylation) are the two residues crucial for SnRK1 enzymatic activity later mutated to generate inactive SnRK1α1 variants. The residues predicted [(Elrouby and Coupland 2010); results in (b)], found by MS/MS analyses [from samples shown in (d)], and confirmed to be crucial for SUMOylation in *E. coli* [results in (e and f)] are indicated. Numbering corresponds to gene model At3g01090.1 according to TAIR. (b to f), SUMOylation assay using the Arabidopsis SUMO machinery reconstituted in *E. coli*. The indicated SnRK1α1 variants harboring 6*His and T7 tags were co-expressed in *E. coli* with the indicated SUMO isoform together with the SUMO-activating (AtSAE1a/AtSAE2) and SUMO-conjugating (AtSCE1) enzymes. GG and AA refer to conjugatable and non-conjugatable SUMO variants, respectively. SUMOylation was assessed by Western-blot using antibodies against the T7-tag. (b) Mutation of predicted SUMOylation sites [“predicted” in (a)]. does not abolish SnRK1α1 SUMOylation. (c) Several residues are SUMOylated in SnRK1α1, as shown by the positive SUMOylation signal with truncated SnRK1α1 variants harboring only the KD or RD. Black and grey arrowheads designate non-SUMOylated and SUMOylated proteins, respectively. (d) SnRK1α1-KD and SnRK1α1-RD samples used to identify the SUMOylated lysine residues [“MS/MS” in (a); their relative position in the

predicted SnRK1 structure is also shown]. SnRK1α1 was purified *via* the His tag by IMAC and immunoblotted against the T7 tag. Bands corresponding to SUMOylated SnRK1α1 (grey arrowhead) were excised and analyzed by MS/MS. RGG denotes mature SUMO3 mutated at the C-terminus (S91R) to generate smaller tryptic peptides more amenable MS/MS analyses. The lysine residues indicated in the table correspond to the ones found to be SUMOylated in MS analyses of SnRK1α1-KD and SnRK1α1-RD using WT mature SUMO3 (GG) or its RGG variant. The structure of the SnRK1 complex in cartoon representation was modeled with the Swiss model portal using the AMPK structure as a template (2Y94). SnRK1α1 is in blue [colored as in (a) with the KA1 domain in dark blue; residues 14 to 395 coupled to a model of the KA1 (Rodrigues *et al.* 2013) from 396 to 512], SnRK1β1 is in yellow (209-281), and SnRK1βγ is in wheat (152-486). SnRK1α1 lysine residues found to be SUMOylated by MS/MS [(a), "MS/MS")] are shown with their sidechains in stick representation in red. The three lysines numbered in red correspond to the three lysines confirmed to be SUMOylated ["confirmed" in (a); see panel (e)]. (e) Same analysis as in (c) on total soluble protein extract from bacteria expressing the indicated SnRK1α1 domains mutated or not for the shown lysines. An area pointed out with a blue arrowhead indicates where the SUMOylated protein should be in the mutated variant (compare to grey arrowhead in the WT control of the same panel). (f) Validation of the mutational analysis in (e) using affinity-purified protein from bacteria expressing a full length SnRK1α1 mutated or not for the three confirmed lysines (K34/63/390). KD, Kinase domain; RD, Regulatory Domain; KA1, Kinase Associated 1 domain; UBA, Ubiquitin-Associated domain. Equal protein loading in (e-f) is shown by Coomassie Blue (CB) staining of membranes.

Figure S5. Salicylic acid (SA) has no effect on SnRK1 signaling

(a) SA does not alter SnRK1 reporter gene induction in protoplasts. The *pDIN6::LUC* reporter for SnRK1 signaling is strongly induced by SnRK1α1 expression, but this induction is similar in mock- and SA-treated cells. Protoplasts were transfected with a plasmid expressing SnRK1α1 or control DNA, incubated for 4h and thereafter treated with SA (5µM) or ethanol (mock control) and the t0 was collected. After 2h or 15h the cells were collected for luciferase activity assays and western-blot (WB). Equal protein loading in (e-f) is shown by Coomassie Blue (CB) staining of membranes. Data presented are means and error bars are SEM (n=3). (b) Various SA treatments induce the

expression of two marker genes of Systemic Acquired Resistance (SAR; *PR1*, At2g14610 and *PR5*, At1g75040), but not the induction of the SnRK1 marker genes *DIN6* (At3g47340), *AXP* (At2g33830), and *TPS8* (At1g70290). The data are from four independent studies and were obtained by using Genevestigator (https://genevestigator.com/gv/).

Figure S6. Specificity of the anti-SnRK1βγ antibody

Several SnRK1βγ-containing protein preparations were used to assess the specificity of the antibody (Agrisera AS09 463) in western-blot ("WB"). The antibody recognized the recombinant protein produced in *E. coli* ("His-SnRK1βγ", presented in Figure 1a) and the HA-tagged protein overexpressed in protoplasts ("SnRK1βγ-HA"). This antibody was also able to recognize SnRK1βγ from SnRK1α1 immunoprecipitation ("IP-SnRK1α1"). However, this antibody fails to recognize SnRK1βγ in crude extracts ("CE"), where only unspecific bands of higher or smaller molecular weight are detected. Arrowhead indicates SnRK1βγ.

Figure S7. Conservation in SnRK1α1 of the residues implicated in SNF1 SUMOylation

(a) Partial ClustalW alignment of the α-subunits of SnRK1 (α1/α2 from Arabidopsis), AMPK (α1/α2 from Human), and SNF1 (*S. cerevisiae*). The two partially overlapping SIMs from SNF1 (Simpson-Lavy and Johnston 2013) are boxed. Only SIM1 (black box, containing I128, pointed) was shown to be important for the inhibition of Snf1 by SUMOylation. (b) Structural alignment of the KA1 domain from Arabidopsis SnRK1α1 [model, pale green, (Rodrigues *et al.* 2013)] and the crystal structure of SNF1 (light blue, PDB: 2QVLA: 506-591). RMS=0.45Å (69 to 69 atoms) generated by Pymol.

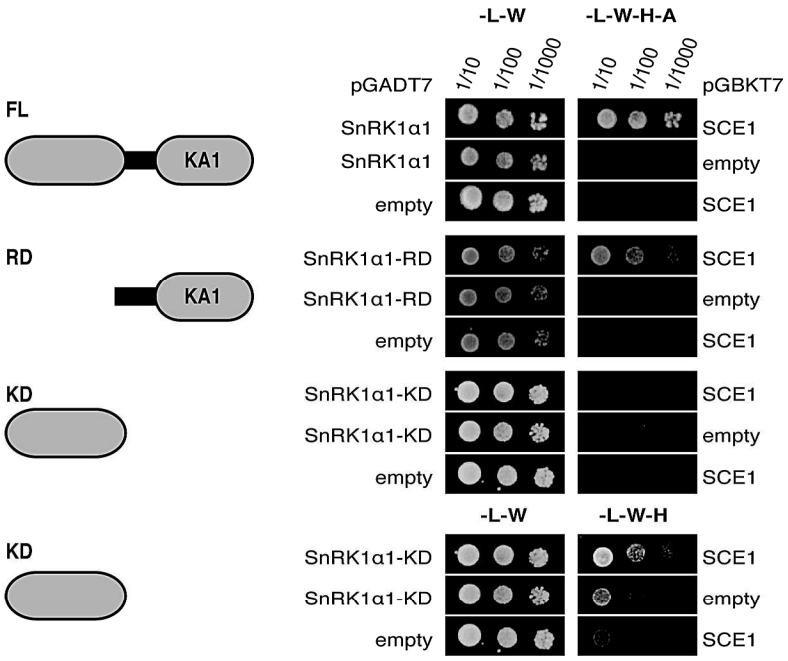

Figure S1. SnRK1α1 interacts with the SUMO E2 Conjugating Enzyme 1 (SCE1) in a Yeast two-Hybrid assay

The full-length coding sequence (FL), C-terminal Regulatory Domain (RD) encompassing the KA1 domain, or N-terminal Kinase Domain (KD) of SnRK1α1 (represented on the left), were cloned into pGADT7 in fusion with the GAL4 activation domain and co-transfected with pGBKT7 harboring either the GAL4 binding domain alone (empty) or in fusion with the full-length SCE1. The growth of transformed AH109 yeast cells was assessed in permissive [-Leucine (L), -Tryptophan (W)], selective [-L-W,-Histidine (H)], or more stringent [-L-W-H,-Adenine (A)] media. A representative experiment of a minimum of two independent assays is shown.

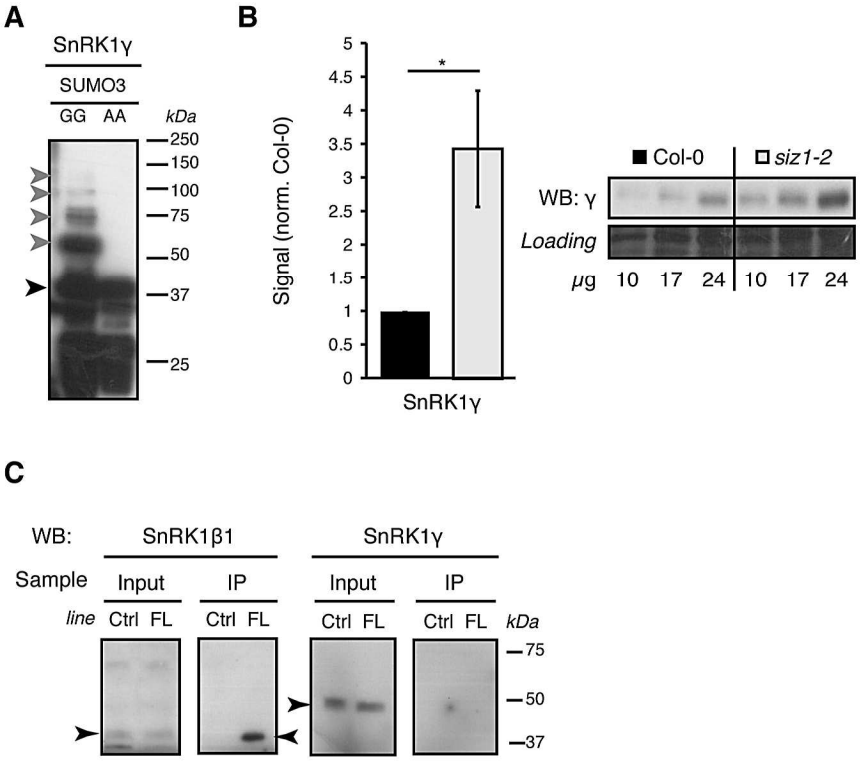

Figure S2. SnRK1γ is SUMOylated in *E. coli* and enriched in *siz1-2*, but is not part of the SnRK1α1 complex in Arabidopsis leaves

(A) SnRK1γ subunits containing 6*His and T7 tags were co-expressed in *E. coli* with SUMO3 together with the SUMO-activating (AtSAE1a/AtSAE2) and SUMO-conjugating (AtSCE1) enzymes. After production, the protein from total lysate was immunoblotted against its T7 tag. GG and AA refer to conjugatable and non-conjugatable SUMO3 variants, respectively. Black and grey arrowheads mark non-SUMOylated and SUMOylated SnRK1γ, respectively.

(B) SnRK1γ accumulates to higher levels in the *siz1-2* mutant. Total leaf protein extracts (10, 17, or 24 μg) of Col-0 and *siz1-2* plants were analyzed by Western-blot (WB) using antibodies against SnRK1γ. The signals were quantified and normalized to loading. The average quantification in *siz1-2* normalized to Col-0 is presented. Stars denote statistical significance, as determined by ratio paired *t*-test prior to normalization (n=3; error bars=SEM; *p<0.05).

(C) Anti-GFP immunoprecipitation (IP) of SnRK1α1-GFP as in Figure 1B. The presence of SnRK1γ was assessed by immunodetection with SnRK1γ antibodies. Co-immunoprecipitation of SnRK1β1 was used as a positive control. The input corresponds to the soluble protein extracts that were used for IP. The black arrowheads indicate the SnRK1 subunits.

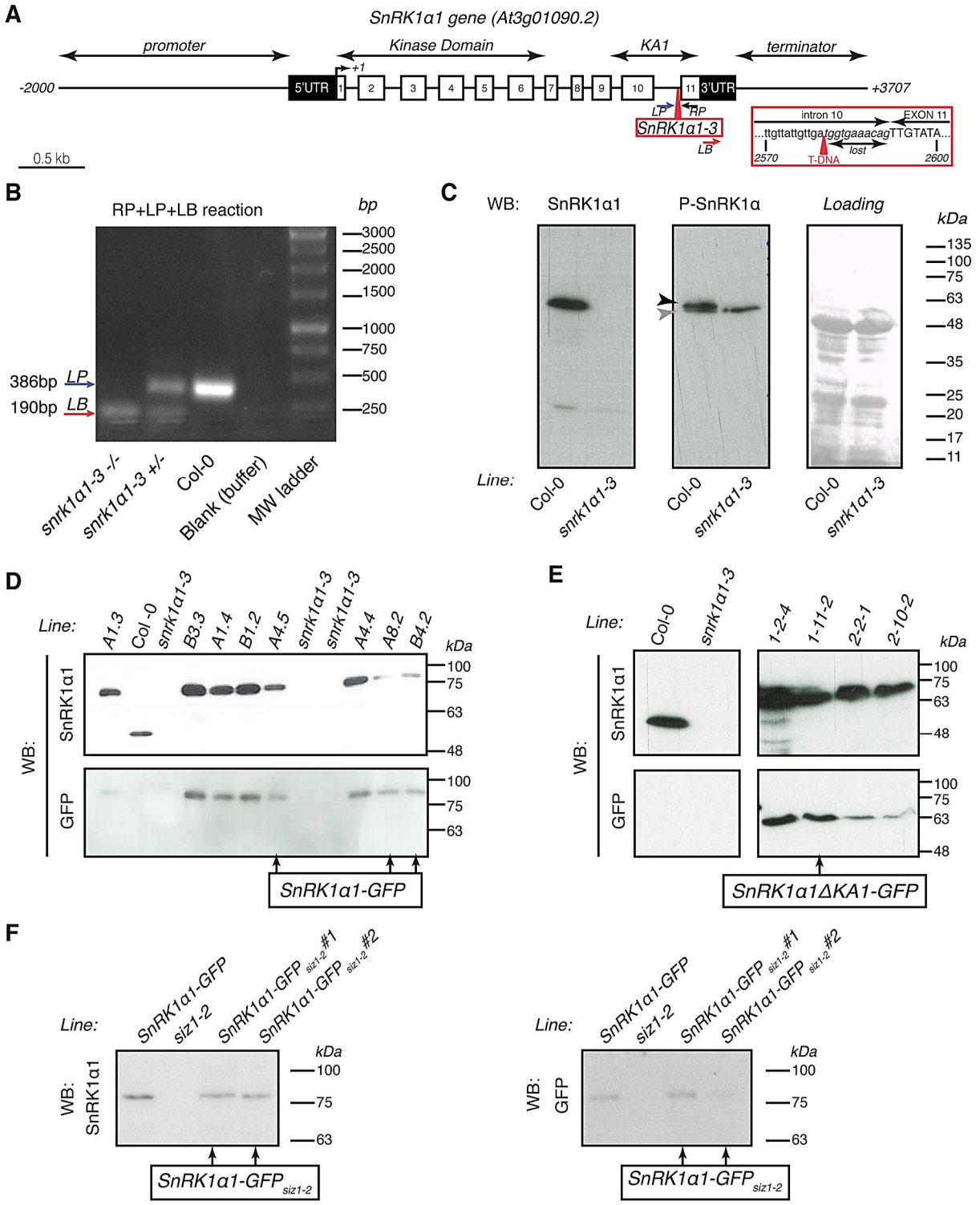

Figure S3. Generation of SnRK1α1-GFP transgenic lines

(A) Structure of the *SnRK1α1* gene (At3g01090.2 gene model). All indicated positions have the start codon (noted +1) as a reference. The promoter (2kb upstream of the start codon) and terminator (1 kb downstream of the stop codon) regions used, as well as the kinase and KA1 domains, are indicated. The location of the T-DNA insertion defining the *snrk1α1-3* mutant line (GABI-KAT: 579E09) is indicated as well as the position of the three genotyping primers (LP, Left Primer; RP, Right Primer; LB, Left Border; Supplementary Table 1). The sequence providing the exact location of the insertion (2583) in indicated inside the red box ("lost" denotes the 11 bases lost due to the insertion). White boxes correspond to exons.

(B) Genotyping PCR using primers LP, RP, and LB, shown in (A). The expected sizes of the two products are indicated on the left (LP: LP-RP reaction, 386bp indicates WT allele; LB: LB-RP reaction, 190bp indicating a mutant allele).

(C) Total proteins from adult Arabidopsis leaves of Col-0 or the *snrk1α1-3* mutant were analyzed by Western blot (WB) using antibodies against SnRK1α1, SnRK1α2 or P-AMPK (recognizing the phosphorylated T175/176 of SnRK1α1/α2, respectively). The black and grey arrowheads indicate phospho-SnRK1α1 and phospho-SnRK1α2, respectively. Equal sample loading is shown by Coomassie staining of the membrane ("loading").

(D) Supporting data for Figure 1B. SnRK1α1::GFP transgenic lines were generated by transformation of the *snrk1α1-3* mutant with the pBm43GW,0 MultiSite Gateway Binary vector, containing the promoter (2 kb upstream of the start codon), the genomic coding region (exons-introns) and the terminator (1 kb downstream of the stop codon) of the *SnRK1α1* gene (At3g01090.2; indicated in (A). Several transformants were tested for the presence of SnRK1α1-GFP by Western-blot (WB) using antibodies against SnRK1α1 and GFP. The selected lines (presenting a SnRK1α1 signal close to Col-0) are indicated with arrows.

(E) *SnRK1α1ΔKA1::GFP* transgenic lines were generated using the CDS of SnRK1α1 and analyzed as in (D).

(F) Supporting data for Figure 2B. *SnRK1α1::GFP*$_{siz1-2}$ transgenic lines were generated by transformation of the *siz1-2* mutant with the pBm43GW,0 MultiSite Gateway Binary construct described in (D). Several transformants were tested for the presence of SnRK1 α1-GFP by Western-blot (WB) using antibodies against SnRK1α1 and GFP. The selected lines are indicated with arrows.

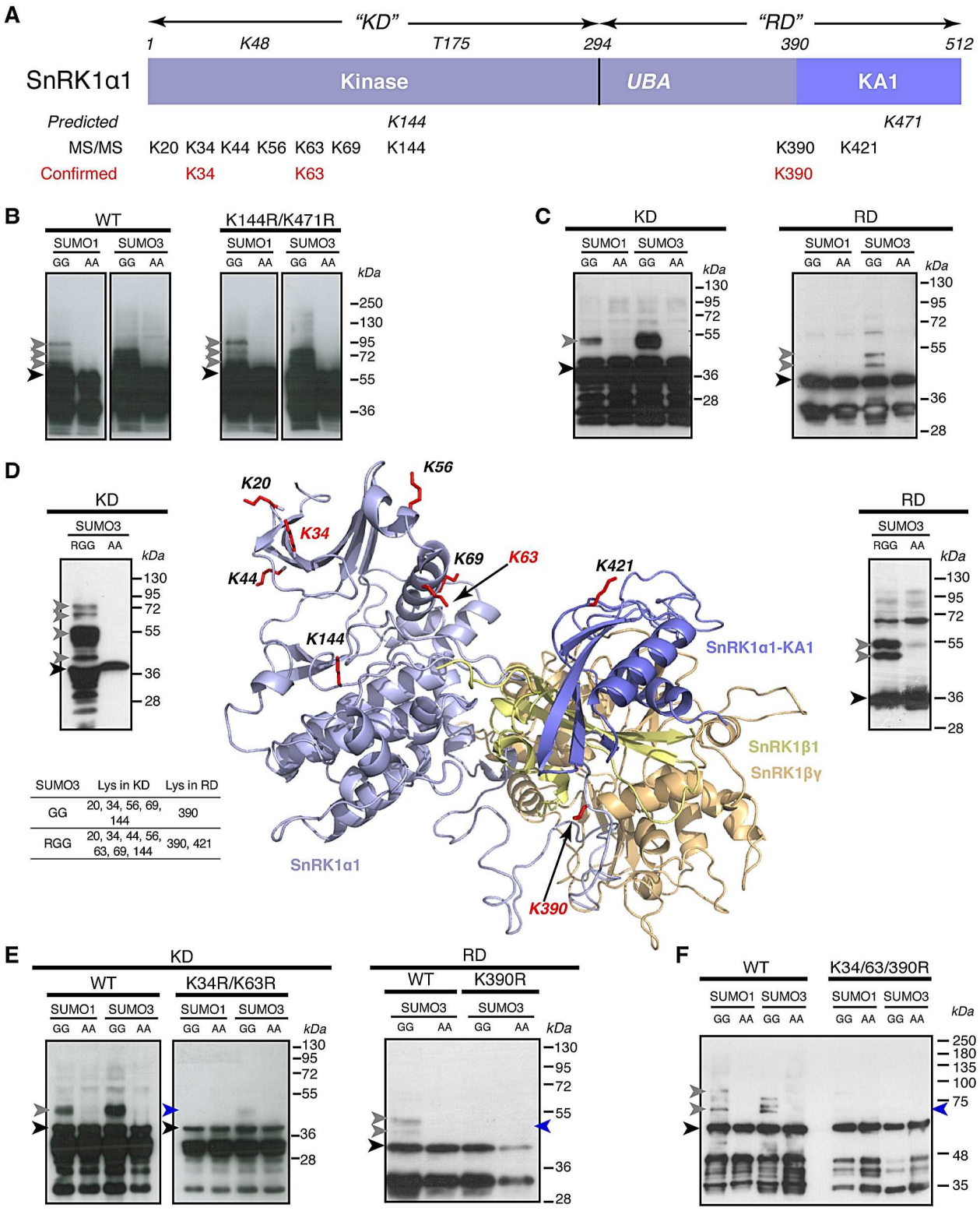

Figure S4. SnRKα1 residues found SUMOylated in the *E. coli* assay

(A) Schematic representation of SnRK1α1 showing the regions referred thereafter. K48 (catalytic phospho-transfer) and T175 (activating T-loop phosphorylation) are the two residues crucial for SnRK1 enzymatic activity later mutated to generate inactive SnRK1α1 variants. The residues predicted [(Elrouby and Coupland, 2010); results in (B)], found by MS/MS analyses [from samples shown in (D)], and confirmed to be crucial for SUMOylation in *E. coli* [results in (E and F)] are indicated. Numbering corresponds to gene model At3g01090.1 according to TAIR. (B to F), SUMOylation assay using the Arabidopsis SUMO machinery reconstituted in *E. coli*. The indicated SnRK1α1 variants harboring 6*His and T7 tags were co-expressed in *E. coli* with the indicated SUMO isoform together with the SUMO-activating (AtSAE1a/AtSAE2) and SUMO-conjugating (AtSCE1) enzymes. GG and AA refer to conjugatable and non-conjugatable SUMO variants, respectively. SUMOylation was assessed by Western-blot using antibodies against the T7-tag.

(B) Mutation of predicted SUMOylation sites ["predicted" in (A)]. does not abolish SnRK1α1 SUMOylation.

(C) Several residues are SUMOylated in SnRK1α1, as shown by the positive SUMOylation signal with truncated SnRK1α1 variants harboring only the KD or RD. Black and grey arrowheads designate non-SUMOylated and SUMOylated proteins, respectively.

(D) SnRK1α1-KD and SnRK1α1-RD samples used to identify the SUMOylated lysine residues ["MS/MS" in (A); their relative position in the predicted SnRK1 structure is also shown]. SnRK1α1 was purified *via* the His tag by IMAC and immunoblotted against the T7 tag. Bands corresponding to SUMOylated SnRK1α1 (grey arrowhead) were excised and analyzed by MS/MS. RGG denotes mature SUMO3 mutated at the C-terminus (S91R) to generate smaller tryptic peptides more amenable MS/MS analyses. The lysine residues indicated in the table correspond to the ones found to be SUMOylated in MS analyses of SnRK1α1-KD and SnRK1α1-RD using WT mature SUMO3 (GG) or its RGG variant. The structure of the SnRK1 complex in cartoon representation was modeled with the Swiss model portal using the AMPK structure as a template (2Y94). SnRK1α1 is in blue [colored as in (A) with the KA1 domain in dark blue; residues 14 to 395 coupled to a model of the KA1 (Rodrigues *et al.*, 2013) from 396 to 512], SnRK1 β1 is in yellow (209-281), and SnRK1βγ is in wheat (152-486). SnRK1α1 lysine residues found to be SUMOylated by MS/MS [(A), "MS/MS")]

Figure S4-continuation
are shown with their sidechains in stick representation in red. The three lysines numbered in red correspond to the three lysines confirmed to be SUMOylated [“confirmed” in (A); see panel (E)].
(E) Same analysis as in (C) on total soluble protein extract from bacteria expressing the indicated SnRK1α1 domains mutated or not for the shown lysines. An area pointed out with a blue arrowhead indicates where the SUMOylated protein should be in the mutated variant (compare to grey arrowhead in the WT control of the same panel).
(F) Validation of the mutational analysis in (E) using affinity-purified protein from bacteria expressing a full length SnRK1α1 mutated or not for the three confirmed lysines (K34/63/390).
KD, Kinase domain; RD, Regulatory Domain; KA1, Kinase Associated 1 domain; UBA, Ubiquitin-Associated domain.

A

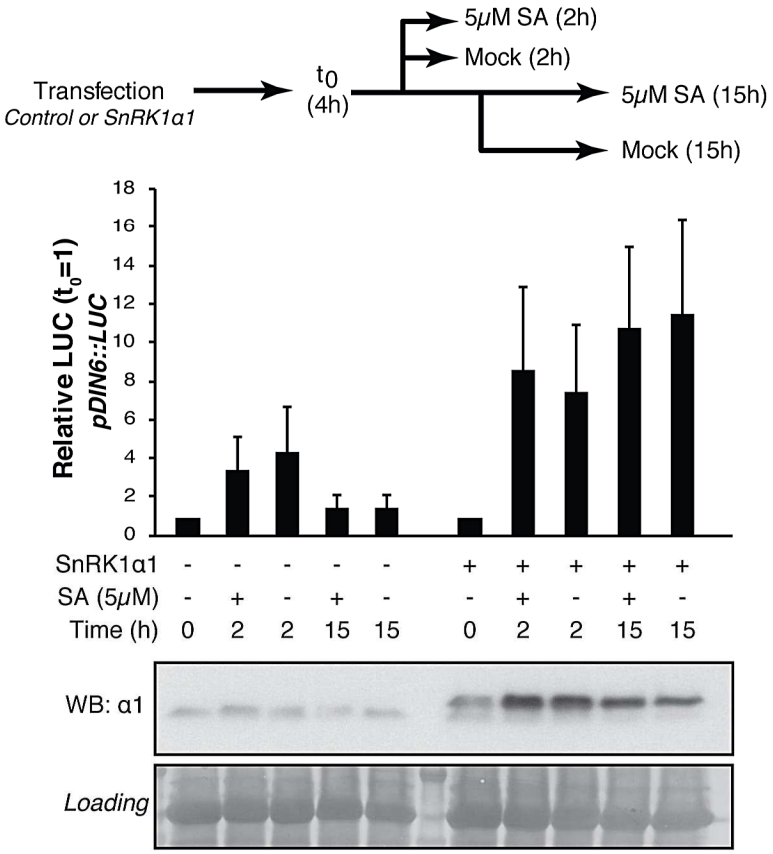

B

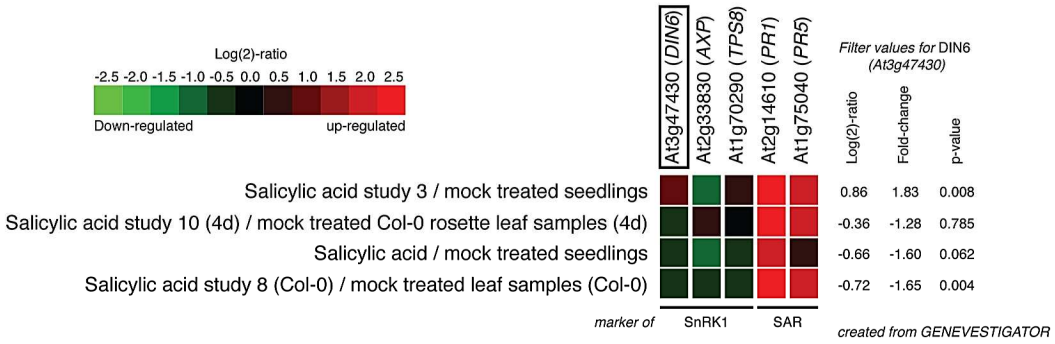

Figure S5. Salicylic acid (SA) has no effect on SnRK1 signaling

(A) SA does not alter SnRK1 reporter gene induction in protoplasts. The *pDIN6::LUC* reporter for SnRK1 signaling is strongly induced by SnRK1α1 expression, but this induction is similar in mock- and SA-treated cells. Protoplasts were transfected with a plasmid expressing SnRK1α1 or control DNA, incubated for 4h and thereafter treated with SA (5μM) or ethanol (mock control) and the t0 was collected. After 2h or 15h the cells were collected for luciferase activity assays and western-blot (WB). Data presented are means and error bars are SEM (n=3).

(B) Various SA treatments induce the expression of two marker genes of Systemic Acquired Resistance (SAR; *PR1*, At2g14610 and *PR5*, At1g75040), but not the induction of the SnRK1 marker genes *DIN6* (At3g47340), *AXP* (At2g33830), and *TPS8* (At1g70290). The data are from four independent studies and were obtained by using Genevestigator (https://genevestigator.com/gv/).

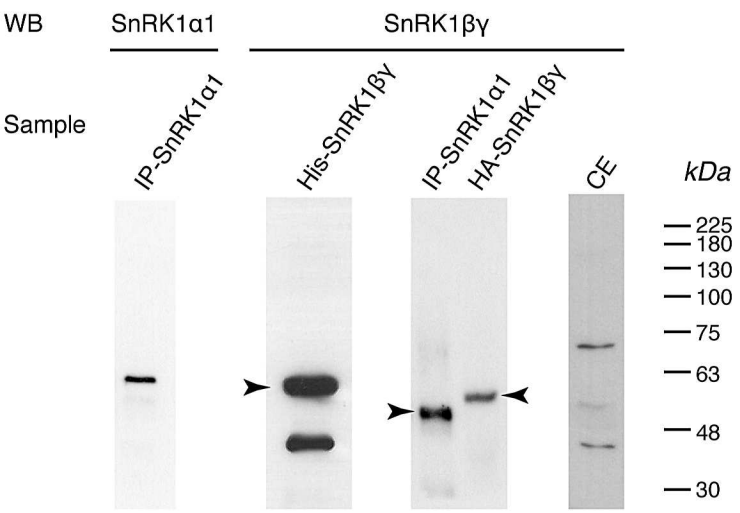

Figure S6. Specificity of the anti-SnRK1βγ antibody

Several SnRK1βγ-containing protein preparations were used to assess the specificity of the antibody (Agrisera AS09 463) in western-blot ("WB"). The antibody recognized the recombinant protein produced in *E. coli* ("His-SnRK1 βγ", presented in Figure 1A) and the HA-tagged protein overexpressed in protoplasts ("SnRK1βγ-HA"). This antibody was also able to recognize SnRK1 βγ from SnRK1α1 immunoprecipitation ("IP-SnRK1α1"). However, this antibody fails to recognize SnRK1βγ in crude extracts ("CE"), where only unspecific bands of higher or smaller molecular weight are detected. Arrowhead indicates SnRK1βγ.

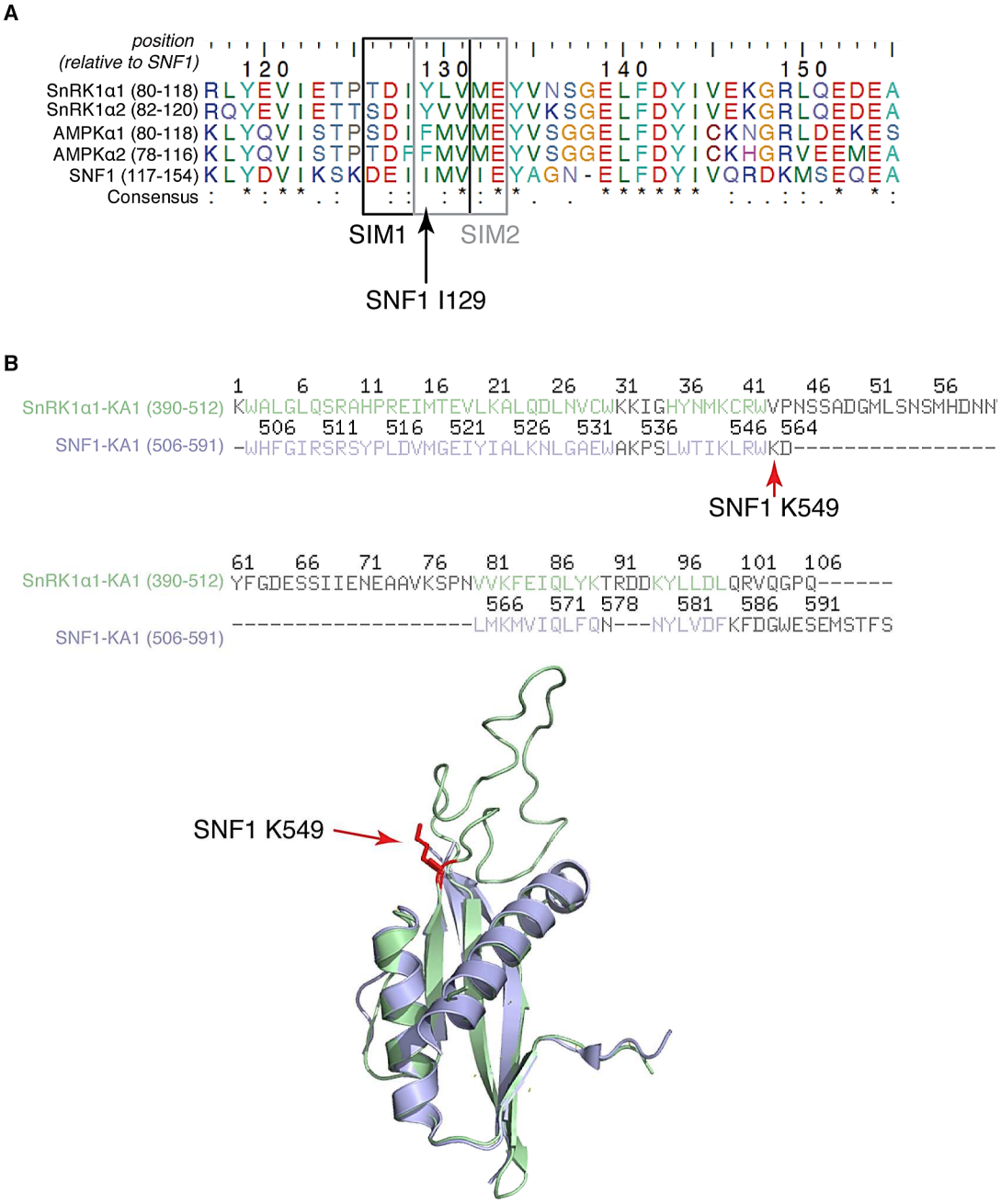

Figure S7. Conservation in SnRK1α1 of the residues implicated in SNF1 SUMOylation

(A) Partial ClustalW alignment of the α-subunits of SnRK1 (α1/α2 from Arabidopsis), AMPK (α1/α2 from Human), and SNF1 (*S. cerevisiae*). The two partially overlapping SIMs from SNF1 (Simpson-Lavy and Johnston, 2013) are boxed.

(B) Structural alignment of the KA1 domain from Arabidopsis SnRK1α1 [model, pale green, (Rodrigues et al., 2013)] and the crystal structure of SNF1 (light blue, PDB: 2QVLA: 506-591). RMS=0.45Å (69 to 69 atoms) generated by Pymol.